Acta Neuropathologica Communications

RESEARCH

Open Access

Overactive EAAT1 Cl^- channels impair GABAergic tonic inhibition in *SLC1A3*-associated episodic ataxia

Yulia Kostritskaia[1,6†], Daniela Bulla-Miely[2†], Miriam Engels[1], Jan Meyer[3], Juliane L. Berns[4], Sabrina Behuet[5], Sebastian Bludau[5], Christine R. Rose[3], Albert Becker[4], Thomas Gensch[1], Ulrike B. S. Hedrich[2†], Christoph Fahlke[1†] and Peter Kovermann[1*†]

Abstract

A missense variant in *SLC1A3*, which results in a proline to arginine substitution in the glial excitatory amino acid transporter 1 (EAAT1), causes a severe form of episodic ataxia type 6, characterized by recurrent attacks of ataxia and epilepsy. EAATs are dual function transport proteins, and the P290R variant reduces secondary active glutamate transport rates, while enhancing the anion channel activity. Here, we used complementary electrophysiological, imaging, biochemical and neuropathological techniques to characterize the cellular mechanisms underlying epileptic seizures in a mouse model of episodic ataxia type 6, the heterozygous $Slc1a3^{P290R/+}$ mouse. Video-EEG recordings demonstrate frequent and severe spontaneous epileptic seizures in vivo. "Gliosis only" phenotype in the cerebrum of $Slc1a3^{P290R/+}$ mice, which was restricted to the hippocampal formation, suggests that this brain structure may be involved in the development of epileptic seizure activity. Electrophysiological recordings from acute slices revealed a reduction in tonic GABAergic transmission in $Slc1a3^{P290R/+}$ dentate gyrus granule cells, and to a lesser extent in cortical layer 2/3 pyramidal neurons before seizure onset. Phasic GABAergic and glutamatergic transmission remained unaltered in juvenile animals of the same developmental stage. There was no difference in expression levels of the $GABA_A$ receptor ($GABA_AR$) δ subunits, suggesting that impaired tonic inhibition results from decreased extrasynaptic GABA concentrations. We identified enhanced GABA uptake by hippocampal radial glia-like cells (RGLs), caused by elevated GABA transporter 3 (GAT-3) expression and by an increased GABA transport driving force—due to lower intracellular chloride levels $[Cl^-]_{int}$ – as cellular basis of impaired tonic inhibition. Our study demonstrates how increased EAAT1 chloride channel activity of the P290R variant can cause hyperexcitability by modifying synaptic GABA concentrations, while impaired EAAT1 glutamate transport leaves glutamatergic synaptic transmission in $Slc1a3^{P290R/+}$ mice unaffected.

Keywords Glutamate transporters, Tonic inhibition, Epilepsy, Dentate gyrus, Radial glia-like cells, Chloride homeostasis

†Yulia Kostritskaia, Daniela Bulla-Miely, Ulrike B. S. Hedrich, Christoph Fahlke and Peter Kovermann contributed to this work.

*Correspondence:
Peter Kovermann
p.kovermann@fz-juelich.de

Full list of author information is available at the end of the article

Introduction

Excitatory amino acid transporters (EAATs) regulate glutamatergic synaptic activity by mediating glutamate uptake into neuronal and glial cells [11, 49, 59]. Beyond their transporter function, EAATs also operate as chloride channels, with channel opening and closing driven by conformational changes during the glutamate transport cycle [19, 20, 40]. In the past, variants of *SLC1A3* (encoding EAAT1) were associated with episodic ataxia type 6, a disorder characterized by the co-occurrence of ataxia, hemiplegic migraine and epilepsy [7–9, 13, 27, 28]. One *SLC1A3* variant predicts the p.Pro290Arg (P290R) substitution that markedly enhances EAAT1 anion channel activity while simultaneously impairing glutamate transport [26, 57, 63]. A knock-in mouse model (*Slc1a3*$^{P290R/+}$) carrying the heterozygous P290R variant in the rodent EAAT1 homologue, the glutamate aspartate transporter (GLAST), recapitulates the neurological symptoms observed in the corresponding human patient [37]. In contrast, homozygous knock-out animals (*Slc1a3*$^{-/-}$) exhibit only mild ataxia [56, 62], supporting the idea that epilepsy in episodic ataxia type 6 is triggered by a gain-of-function in EAAT1 anion channel activity, rather than by impaired glutamate transport. Ataxia in *Slc1a3*$^{P290R/+}$ mice was recently shown to be caused by Bergmann glia apoptosis, which is triggered by increased glutamate-activated chloride (Cl^-) efflux during infancy and leads to cerebellar degeneration [37]. However, cerebellar degeneration cannot account for the severe epileptic phenotype of *Slc1a3*$^{P290R/+}$ mice. Outside the cerebellum, EAAT1 and its rodent homologue GLAST are highly expressed in hippocampal radial glia-like cells (RGLs), a population of glial stem cells in the subgranular zone of the dentate gyrus (DG) that can differentiate into either granule neurons or astrocytes [4, 30]. Since RGLs are functionally and spatially coupled to granule cells [46], functional changes in EAAT1/GLAST might modify synaptic transmission in DG neurons and contribute to network dysfunction. To understand the cellular basis of epilepsy in *Slc1a3*$^{P290R/+}$ animals, we characterized the epileptic phenotype in vivo and studied neurotransmission in hippocampal and cortical neurons in vitro using electrophysiological, imaging, biochemical and histological approaches.

Material and methods

Animals

WT (wildtype) and heterozygous (*Slc1a3*$^{P290R/+}$) mice of both sexes from the 129 substrain 129S6/SvEvTac (Taconic Biosciences) were used for experiments conducted between P10 and P100. Animals were maintained under a 12-h light/dark cycle with ad libitum access to food and water. The common health status was monitored regularly 4 times per year. Each *Slc1a3*$^{P290R/+}$ mouse was assessed 2 × per week, starting from P15, with a scoring system and euthanasia criteria, which were proofed by the use commitees in North-Rhine Westphalia and Baden Württemberg. For more detail, please refer to Supplementary material.

In vivo video-EEG monitoring

Male *Slc1a3*$^{P290R/+}$ and WT animals were implanted with wireless EEG transmitters (ETA-F10 or HD-X02, Data Sciences International (DSI)) during two developmental time windows: P25-P32 (before seizure onset: $N = 5/5$) and P44-P53 (after seizure peak: $N = 8/10$, WT/*Slc1a3*$^{P290R/+}$). A minimum body weight of 14 g (juvenile group) and 20 g (older group) was required. Anaesthesia was induced either by a single intraperitoneal injection of fentanyl (5 mg/kg, Dechra Veterinary Products Deutschland GmbH), midazolam (5 mg/kg, hameln pharma Gmbh) and medetomidine (0.5 mg/kg, Zoetis Inc.), also referred to as 3-component-anaesthesia, or by 1.5% isoflurane (CP Pharma Handelsgesellschaft mbH) in O_2 via a face mask, with buprenorphine (0.1 mg/kg, CP Pharma Handelsgesellschaft mbH) administered for analgesia. Only the younger group received anaesthesia with buprenorphine. Carprofen (5 mg/kg, Zoetis Deutschland GmbH) was administered intra- and postoperatively. Animals were positioned in a stereotaxic frame equipped with a heating pad (Stoelting Co.). Small holes were drilled to expose the dura and electrodes were placed directly onto its surface (1 mm anterior to bregma, 1 mm lateral), then secured with dental cement (Supplementary Fig. S1a). The transmitter was positioned in a lateral subcutaneous pocket. Antagonisation of anaesthesia was achieved using naloxone (1.2 mg/kg, hameln pharma GmbH), atipamezole (2.5 mg/kg, Dechra Veterinary Products Deutschland GmbH) and, in older mice only, flumazenil (0.5 mg/kg, Fresenius Kabi Deutschland GmbH). Anaesthesia with buprenorphine was not antagonised.

Video-EEG monitoring was initiated 3–7 days post-surgery, or earlier if seizures were suspected, and recordings were performed between P25–P32 (juvenile group) and P44–P53 (older group). Monitoring was performed in a suitable undisturbed environment. In the younger group, the average EEG recording duration per heterozygous animal was 37.0 h for mice receiving the 3-component-anaesthesia and 46.9 h receiving the buprenorphine anaesthesia. In this group, the average EEG recording duration of the respective WT littermates was comparable. In the older group, the average recording duration per animal was 49.7 h for WT and 37.8 h for heterozygous mice. The difference in recording times reflects the higher mortality rate in the *Slc1a3*$^{P290R/+}$ group. Despite this, the total recording duration was similar between genotypes (WT: 347.6 h, *Slc1a3*$^{P290R/+}$: 378.4 h). One

WT mouse died postoperatively, but the cause of death remained unclear. Mice were monitored in their home cages (PhysioTel receiver, Ponemah software, DSI; Noldus software, Noldus Information Technology BV), with sampling rates of 1.0 kHz (ETA-F10) or 0.5 kHz (HD-X02). EEG analysis was performed using Neuroscore software (DSI). Seizures were defined as rhythmic discharges lasting > 10 s and < 5 min, with or without behavioural manifestations. Status epilepticus was defined as seizure activity > 5 min or recurrent seizures without full recovery.

Following the experiment, animals were euthanised by intraperitoneal injection of ketamine (150 mg/kg, Wirtschaftsgenossenschaft deutscher Tierärzte eG) and xylazine (15 mg/kg, Albrecht GmbH).

Neuropathology and immunostainings

For microscopic analyses, mouse brain tissues were fixed with paraformaldehyde overnight. For paraffin sections, brains were embedded into paraffin after dehydration with a series of increasing [EtOH] and Rotihistol (Sigma-Aldrich, Merck). 4 µm sections were used for both, hematoxylin–eosin (HandE) staining and immunohistochemistry by using standard protocols. Briefly, paraffin sections were de-paraffinised in xylene for 10 min followed by decreasing alcohol series (100–50%) for 2 min each. After washing, slides were subjected to a citric acid antigen retrieval procedure with inactivation of endogenous peroxidases by incubation in a solution containing (in mM): 21 $C_6H_8O_7$, 6 Na_2HPO_4, and 15% (v/v) H_2O_2 (15 min, RT). Antigen retrieval was performed by boiling the sections for 20 min in Tris–EDTA-buffer (2 Tris, 0.063 EDTA, pH 8.0). Subsequently, brain sections were rinsed for 2 h at 37 °C in PBS blocking buffer (10% normal goat serum). Slices were washed and incubated with antibodies against glial fibrillary acidic protein (GFAP, Sigma, 1:500) overnight at 4 °C. After washing, slices were incubated with respective biotinylated secondary antibodies (Vector Laboratories, USA, 1:200) in blocking buffer and incubated for 2 h at 37 °C. Slides were again washed and further processed according to manufacturer's protocol (Sigma-Aldrich) and mounted with Mowiol 4–88 (Carl Roth GmbH).

Immunostainings of cryo-protected tissues for confocal microscopy were prepared as followed: Brains were immersion-fixed in 4% PFA in phosphate buffer (PB; in mM: 81 $NaH_2PO_4{\cdot}2H_2O$, 9 $Na_2HPO_4{\cdot}H_2O$, pH 7.4) for 30 min at 4 °C, followed by washing in PB for 30 min at RT. Cryoprotection was achieved by sequential incubation in PB containing 10% sucrose (1 h, RT) and 30% sucrose (overnight, 4 °C). Hemispheres were embedded in NEG-50 frozen section medium (Thermo Fisher Scientific) and sectioned sagittally at 14 µm using an HM560 cryotome (Thermo Fisher Scientific). Non-specific binding was blocked overnight at 4 °C in 1% (w/v) bovine serum albumin in PB. Frozen and paraffin sections were incubated overnight at 4 °C with primary antibodies against brain lipid-binding protein (BLBP), integrin α-M (CD11b), GABA transporter-3 (GAT-3), glial fibrillary acidic protein (GFAP), or Glutamate-Aspartate transporter (GLAST) (RRIDs: AB_10000325, AB_2650514, AB_304437, AB_1556315, AB_10829302), followed by incubation with cyanine dye-conjugated secondary antibodies (RRIDs: AB_2340370, AB_2340460, AB_2340612, AB_2340813) for 45 min at RT. All antibodies were diluted in PB supplemented with 5% ChemiBLOCKER (Merck Millipore) and 1% Triton X-100. RGLs were quantified by counting cells positive for three proteins (BLBP, GLAST, and GFAP) in individual confocal planes. GAT-3 fluorescence intensity was normalised to the BLBP fluorescence intensity per cell for analysis in Fig. 4j

Whole-cell patch clamp recordings

For electrophysiological analyses, mice of both sexes, either prior to the paroxysmal period between P15 and 25, or after seizure onset at P40, were deeply anesthetized with isoflurane and rapidly decapitated. Brains were immediately transferred to ice-cold Ringer's solution A (in mM: 125 NaCl, 2.5 KCl, 1.25 NaH_2PO_4, 26 $NaHCO_3$, 0.5 $CaCl_2$, 5 $MgCl_2$, 20 $C_6H_{12}O_6$; bubbled with 5% CO_2/95% O_2). Parasagittal 250 or 260 µm-thick slices and coronal 350 µm-thick slices were prepared using vibratomes (υ = 60/90 Hz, amplitudes = 1.0/0.9 mm; 7000 SMZ2 (Campden Instruments)/Microm HM650V (Thermo Fisher Scientific)). Slices were transferred to oxygenated Ringer's solution B (125 NaCl, 2.5 KCl, 1.25 NaH_2PO_4, 26 $NaHCO_3$, 2 $CaCl_2$, 1 $MgCl_2$, 25 $C_6H_{12}O_6$) for recovery: 30 min at 37 °C followed by 90 min at RT for parasagittal slices and 60 min at 37 °C for coronal slices.

Whole-cell patch-clamp recordings from neurons in the hippocampus and in neocortical layer 2/3 were performed in acute brain slices, using either an EPC10-USB amplifier (RRID: SCR_018399) with PATCHMASTER software (HEKA Elektronik, RRID: SCR_000034) or a Multiclamp 700B amplifier (RRID: SCR_018455) and DigiData 1420 with pClamp 10.6 software (Molecular Devices, RRID: SCR_011323). Recordings were conducted at RT (hippocampus) or 34 °C (cortex) with constant perfusion of Ringer's solution B supplemented with 50 µM (2*R*)-amino-5-phosphovaleric acid (AP-5) (Tocris Bioscience). Patch pipettes were filled with intracellular solution containing (in mM): 130 CsCl, 8 NaCl, 0.2 $MgCl_2$, 2 EGTA, 4 Mg-ATP, 0.3 Li-GTP, 1 QX-314, and 10 HEPES (pH 7.2, adjusted with CsOH). Cells were voltage-clamped at -70 mV.

GABAergic mIPSCs and tonic GABA currents were recorded in the presence of 1 µM tetrodotoxin (TTX)

(Tocris Bioscience) and 10 µM cyanquixaline (CNQX) (Tocris Bioscience). Tonic $GABA_AR$-mediated conductance was quantified by comparing the mean holding current over 30 s before and after 3 min application of 50 µM PTX. α-amino-3-hydroxy-5-methyl-4-isoxazolepropionic acid (AMPA) receptor-mediated mEPSCs were recorded in the presence of 1 µM TTX and 100 µM picrotoxin (PTX) (Tocris Bioscience). Whole-cell patch-clamp recordings of electrogenic GABA-uptake currents in DG RGLs were performed in acute slices (260 µm) from P19-P23 mice. To isolate GABA-uptake currents, Ringer B solution was supplemented with 100 µM PTX and 1 µM 3-(1-(3,4-dichlorophenyl)ethyl)amino-2-hydroxypropyl-phenyl-methyl-phosphinicacid-hydrochloride (CGP55845) to block $GABA_A$ and $GABA_B$ receptors, respectively. Patch pipettes were filled with two different intracellular solutions containing different Cl^- concentrations ($[Cl^-]$) based on the mean values obtained from FLIM microscopy of DG RGLs (WT: 20.8 mM KCl; P290R/+: 18 mM KCl). Equimolar substitution was performed to achieve a final potassium concentration ($[K^+]$) of 140 mM using potassium methanesulfonate (K-Met-SO_4) (Sigma-Aldrich) (in mM, WT: 119.2 K-Met-SO_4/20.8 KCl; P290R/+: 122 K-Met-SO_4/18 KCl; both genotypes: 2 Mg-gluconate, 1 Ca-gluconate, 3 Mg-ATP, 2 Na-GTP, 10 HEPES–KOH, pH 7.4). Acute slices were incubated with 2 µM sulforhodamine 101 (SR101) (Sigma-Aldrich) for 20–30 min at 37 °C to label RGLs, followed by a 20 min incubation in dye-free Ringer B solution, and visualised using infrared microscopy (Slicescope, Scientifica). GABA uptake responses of RGLs held at -70 mV were evoked by brief puff applications (5 s) of Ringer B solution containing 0.5 mM GABA, $GABA_A$- and $GABA_B$ blockers, using a pneumatic drug ejection system (PDES-DXH, npi electronic GmbH). Maximum response amplitudes were recorded in individual cells, averaged per cell and then pooled across animals (*N*) for statistical analysis.

Sodium imaging of RGLs

Sodium imaging was performed on brain slices from male and female mice aged P22 to P27 that had no prior history of overt seizures. Detailed informations about intracellular sodium imaging and the technical equipment is provided in Supplementary material.

Fluorescence lifetime imaging microscopy

We measured $[Cl^-]_{int}$ in hippocampal astrocytes and RGLs in acute brain slices from animals between P20 and P30 (prior and at the beginning of overt seizure onsets), using fluorescence lifetime imaging (FLIM) and the Cl^- sensitive quinolinium dye 1-(ethoxycarbonylmethyl)-6-methoxyquinolinium bromide (MQAE) (Sigma-Aldrich). Detailed information about the used technical equipment is provided in the Supplementary material. The mean fluorescence lifetimes were determined using multidimensional time-correlated single-photon counting (TCSPC, Simple-Tau 152; Becker and Hickl) with a volume of 0.08 mm^3 per individual pixel, resulting in a three-dimensional resolution of approximately 1.3 mm in the z-axis and 0.35 mm in the x- and y-axis [67]. Prior to imaging, acute brain slices were incubated in oxygenated Ringer's solution A containing 2 µM SR101 for 20 min at 37 °C, followed by a ten-minute incubation in SR101-free oxygenated Ringer's solution B to stain astrocytes and RGLs. After 30 min at RT, slices were incubated with MQAE (3.5 mM, Sigma-Aldrich, Merck) in Ringer's solution B for 30 min. MQAE fluorescence is collisionally quenched by Cl^- ions, resulting in a linear relationship between the inverse fluorescence lifetime and $[Cl^-]_{int}$ [32, 60]:

$$\frac{\tau_0}{\tau} = 1 + K_{SV} \quad [Cl^-]_{int}$$

where τ is the MQAE fluorescence lifetime at a given $[Cl^-]_{int}$, τ_0 is the MQAE fluorescence lifetime in the absence of Cl^-, and K_{SV} is the cell type-specific Stern–Volmer constant. After calibration in astrocytes and RGLs [18] using the two-ionophore calibration method [32, 38], the $[Cl^-]_{int}$ for individual cell somas was calculated from the mean fluorescence lifetime of all pixels within the region of interest. To block EAAT1/GLAST activity, slices were incubated in Ringer's solution B supplemented with 20 µM of the EAAT1/GLAST blocker UCPH-101 (Abcam) for 20 min.

Western blotting

For details on Western blotting procedures and used antibodies, please refer to Supplementary Material.

Quantitative receptor autoradiography

Quantitative receptor autoradiography was performed as previously described [66] using animals of both sexes after the paroxysmal period at P50. For further details, please refer to Supplementary material.

Dendritic spine quantification

Golgi–Cox staining was performed following established protocols [48]. The analysis was done with the open-source software Synapse Web Reconstruct (RRID: SCR_002716). For details on analysis, please refer to Supplementary material.

Statistical analysis

Statistical analyses were performed using SigmaPlot (Systat Software GmbH, RRID: SCR_003210), Microcal-Origin (OriginLab; RRID: SCR_002815) or GraphPad Prism 9.5.1 (GraphPad Software, RRID: SCR_002798). Unless

stated otherwise, data are presented as boxplots, where the box represents the interquartile range (IQR: 25th to 75th percentile), the horizontal line indicates the median and the black squares indicate the data means. Whiskers span the minima and maxima of means within animals (*N*). No outliers were excluded from the analysis. For patch-clamp recording and $[Cl^-]_{int}$ data, individual cells (*n*) are plotted as small symbols, while animal-level averages (*N*) are indicated by larger symbols. In the main text, $[Cl^-]_{int}$ are reported as means ± SD, calculated from individual animal averages. Datasets with normal distributions were compared using *one* or *two-way* ANOVA with Holm–Šidák, Bonferroni or Tukey post hoc tests or in case of single dual datasets with *two-tailed t*-tests. Non-normally distributed data, as determined by Shapiro–Wilk or Kolmogorov–Smirnov-tests, were analysed using Kruskal–Wallis ANOVA on ranks or Mann–Whitney *U*-tests. *P*-values ≤ 0.05 were considered statistically significant. Wherever feasible, experiments were performed in a blinded manner. However, due to the overt phenotype, particularly in experiments involving older animals (> P15), which had to be monitored regularly, or the use of different genotype-dependent pipette solutions in electrophysiological recordings, blinding of investigators was not always possible. Data supporting this study are freely available at: https://github.com/peterkoverman n/episodic_ataxia_6_II/.

Results

Slc1a3$^{P290R/+}$ mice exhibit severe epilepsy

Slc1a3$^{P290R/+}$ mice exhibit severe epilepsy [37], with disease onset typically occurring during the third postnatal week, and peak seizure susceptibility between three and four weeks. Seizures typically begin with rapid tail movements and head turning, progressing to whole-body stretching and clonic activity, while severe episodes involve tonic–clonic seizures with loss of startle reflexes (Fig. 1a, Supplementary video SV1). Postictal behaviour includes immobility and reduced responsiveness. Due to the severity of the phenotype, many *Slc1a3*$^{P290R/+}$ animals reached predefined euthanasia criteria, primarily due to ongoing seizures or weight loss, preventing accurate mortality quantification. Seizure susceptibility in *Slc1a3*$^{P290R/+}$ animals was associated with significant reductions in body weight (Fig. 1b).

To further characterize the epileptic phenotype, video-EEG monitoring was performed in heterozygous and WT mice during and after peak seizure susceptibility in young (P25-P32) and older (P45-P60) cohorts (young group: *N* = 5/5 mice per subgroup; old group: *N* = 8/10 mice, WT/*Slc1a3*$^{P290R/+}$). The young cohort consisted of two subgroups implanted under either 3-component- or buprenorphine-based anaesthesia (Fig. 1c, Supplementary Fig. 1a), as the initial 3-component regimen resulted in 100% incidence of fatal seizures/status epilepticus. In young *Slc1a3*$^{P290R/+}$ mice, EEG monitoring was initiated within 24 h post-implantation and revealed frequent ictal activity across both anaesthesia regimens during the peak susceptibility window (P25-P32), with differences in frequency and severity (Fig. 1d, e). In the subgroup implanted under 3-component-anaesthesia, all *Slc1a3*$^{P290R/+}$ mice exhibited severe epileptic activity with recurrent seizures and no recovery of consciousness between events. EEG recordings showed profoundly suppressed interictal activity, consistent with continuous status epilepticus (Fig. 1d, Supplementary Fig. 1b). Four *Slc1a3*$^{P290R/+}$ animals reached euthanasia criteria, and one animal died overnight during monitoring, highlighting a high mortality rate during the peak seizure period (Fig. 1f). In contrast, young *Slc1a3*$^{P290R/+}$ mice implanted under buprenorphine-based anaesthesia displayed a milder and more heterogeneous phenotype. Two mice developed prolonged near-continuous status epilepticus, whereas three showed only isolated seizures and/or status events (Fig. 1e, f). Overall, seizure burden and mortality were reduced compared to the 3-component-anaesthesia group, with only two animals reaching endpoint criteria (Fig. 1f). The animals exhibited one to four ictal events (seizures and status epilepticus) per mouse. Individual seizures were rare (one to two per animal; 12 s and 3.6 min, mean 1.5 min), while status epilepticus occurred as discrete or near-continuous episodes (zero to three per animal) lasting 0.26 to 47.70 h.

In the post-peak group (P45-P60), seven out of ten mice exhibited at least one seizure or status epilepticus, while three were seizure-free; six animals reached euthanasia criteria or died during monitoring (Fig. 1f). Compared to younger mice, older animals showed a less severe epileptic phenotype with intermittent seizure or status epilepticus events on EEG (Fig. 1g). The number of ictal events per *Slc1a3*$^{P290R/+}$ animal ranged from one to 25 ictal events, with all affected mice experiencing at least one episode of status epilepticus. Seizures lasted on average 48.8 s (range: 12 s to 2.4 min) and occurred one to 15 times per day (mean five). Status epileptici lasted 0.1 to 10.8 h (mean 2.2 h) and were accompanied by prolonged periods of altered consciousness with intermittent convulsive behaviours.

Tonic GABAergic inhibition is impaired in *Slc1a3*$^{P290R/+}$ hippocampal granule cells

To investigate potential mechanisms underlying increased seizure susceptibility in *Slc1a3*$^{P290R/+}$ mice, we examined synaptic transmission in the hippocampus and also in the cortex – two brain regions frequently implicated in the pathogenesis of genetic epilepsies [2]. Epileptic activity is commonly associated with an imbalance between excitation and inhibition, often resulting

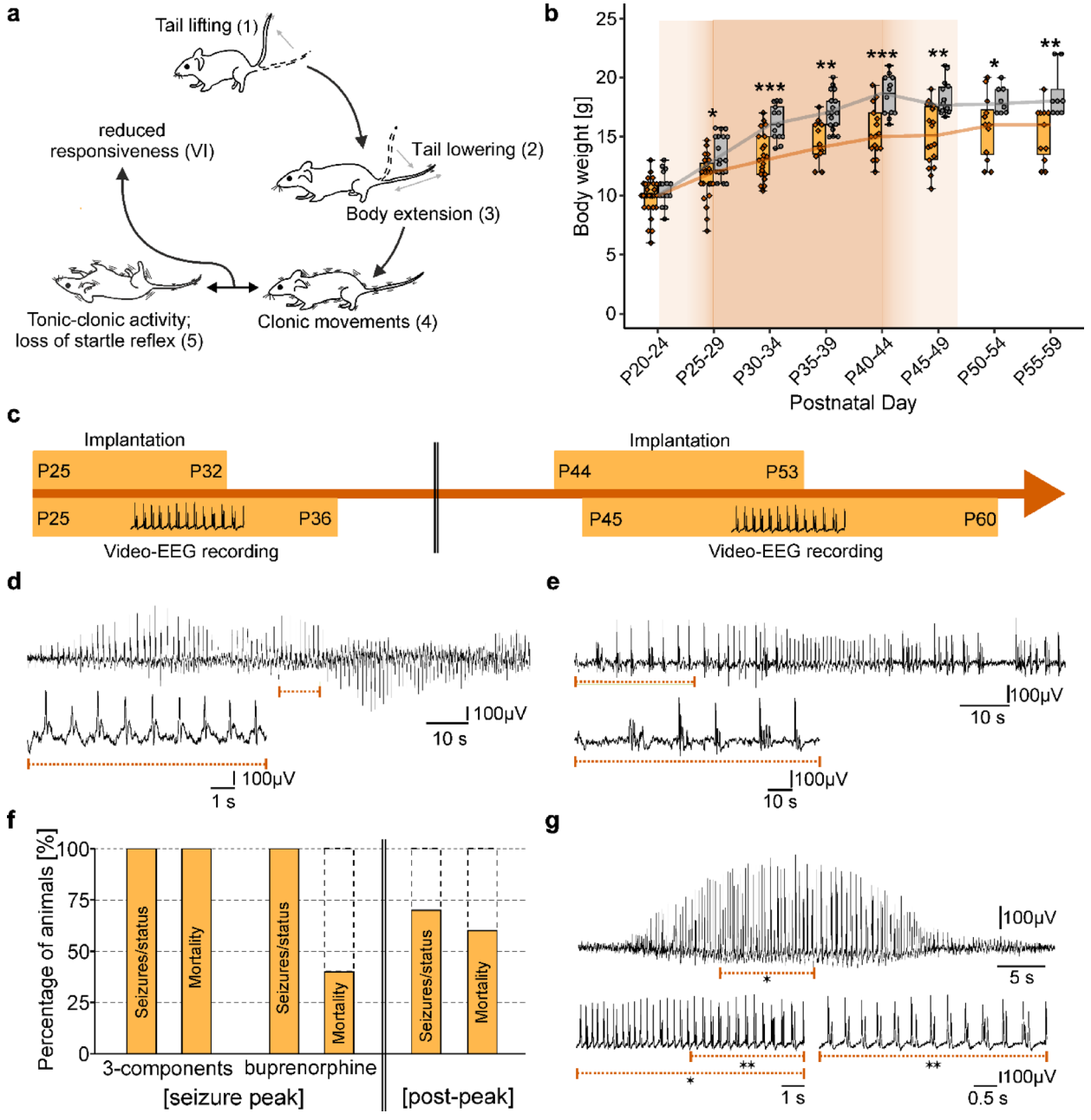

Fig. 1 Seizure burden in *Slc1a3*$^{P290R/+}$ mice changes across development. **a** Sequential stages of seizures, beginning with tail lifting (1) and lowering (2), followed by body extension (3) and clonic movements (4). Severe episodes include tonic–clonic activity and transient loss of startle reflexes (5). Reduced responsiveness occurs postictally (6). **b** Age-dependent changes in body weight of wildtype (WT, grey) ($N=25$) and *Slc1a3*$^{P290R/+}$ (orange, $N=42$) animals; individual mice are shown as small symbols. Shading indicates the seizure peak. **c** Timeline of transmitter implantations and video-EEG monitoring in animals before/during (P25-P36) and after the peak seizure period (P44-P60). **d** Representative EEG trace showing rhythmical spike-and-wave discharges in a P29 mutant animal after implantation under 3-component anaesthesia during seizure peak, with a magnified 10 s segment of the ictal event (cut-out location indicated). **e** Representative EEG trace showing rhythmical spike-and-wave discharges in a mutant animal during seizure peak under buprenorphine-based anaesthesia, with a magnified 10 s segment of the ictal event (cut-out location indicated). **f** Percentage of animals that suffered from seizures/status or died/euthanised in EEG-monitored *Slc1a3*$^{P290R/+}$ mice during seizure peak (3-components and buprenorphine-anaesthesia cohorts) and post-peak period (young group: $N=5$ *Slc1a3*$^{P290R/+}$ animals; older group: $N=10$ *Slc1a3*.$^{P290R/+}$ animals). **g** Representative EEG trace from a mutant animal recorded during a later stage of epileptogenesis, with a gradual increase in spike-and-wave discharge amplitude. Insets display 10 s and 5 s magnifications of the ictal event (cut-out locations indicated)

from impaired $GABA_AR$-mediated inhibition [64]. We therefore performed whole-cell patch-clamp recordings in acute hippocampal and coronal brain slices from WT and heterozygous mice, targeting DG granule cells, CA1 pyramidal neurons, and layer 2/3 pyramidal neurons in the somatosensory cortex. Tonic GABAergic inhibition arises from the persistent activation of extrasynaptic $GABA_ARs$ and plays a critical role in controlling neuronal excitability through Cl^--mediated shunting inhibition and hyperpolarisation [64]. Even subtle alterations in tonic current amplitude can have a substantial impact on neuronal excitability [45]. Tonic GABAergic currents were pharmacologically isolated using the $GABA_AR$ antagonist PTX and quantified as the difference in holding current before and after PTX application (Fig. 2a). In DG granule cells of P20 *Slc1a3*$^{P290R/+}$ mice—prior to the onset of spontaneous seizures—tonic $GABA_AR$-mediated currents were significantly reduced compared

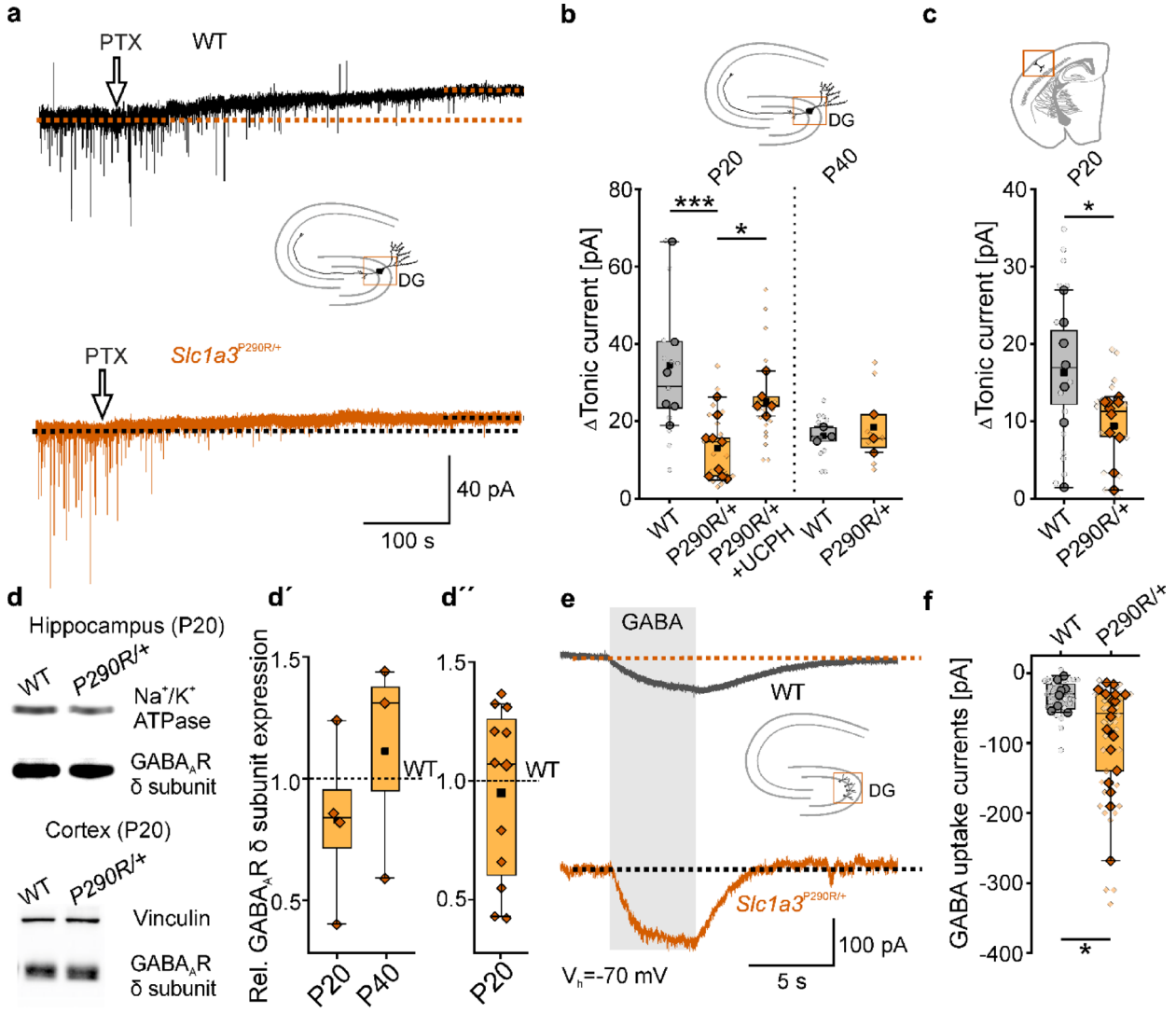

Fig. 2 $GABA_AR$-mediated tonic inhibition is reduced in *Slc1a3*$^{P290R/+}$ dentate gyrus (DG) granule cells. **a** Representative tonic currents recorded from juvenile (P20) WT (top) or *Slc1a3*$^{P290R/+}$ (bottom) DG granule cells with the start of the PTX (50 µM) application marked by an arrow. **b** Mean amplitudes of tonic currents at P20 ($n = 11/18$ *Slc1a3*$^{P290R/+}$/WT cells, $N = 6/9$ animals; $p \leq 0.001$) and P40 ($n = 11/8$, $N = 3/3$, WT/*Slc1a3*$^{P290R/+}$, $p = 0.99$, *two-way* ANOVA, Holm–Šidák post hoc tests). UCPH-101 treatment increases tonic current amplitudes in mutant DG granule cells at P20 ($n = 17$, $N = 5$, *Slc1a3*$^{P290R/+}$, $p = 0.044$). Comparison of WT controls and the *Slc1a3*$^{P290R/+}$ + UCPH-101 group revealed no significant difference ($p = 0.80$). **c** Mean tonic current amplitude of L2/3 cortical pyramidal neurons at P15-P20 ($n = 14/15$, $N = 7/10$, $p = 0.043$; *two-tailed t*-test). **d** Western blots of $GABA_AR$ δ subunit expression in hippocampal and cortical tissues at P20. Na^+/K^+-ATPase and vinculin served as loading controls. The graphs show the ratios of $GABA_AR$ δ subunit expression in *Slc1a3*$^{P290R/+}$ mutant tissues by WT control values for the hippocampus (**d'**, $N = 4/4^{P20}$, $3/3^{P40}$, $p = 0.195^{P20}/0.888^{P40}$) and for the cortex (**d''**, $N = 12/11^{P20}$, WT/*Slc1a3*$^{P290R/+}$, $p = 0.115$, *two-tailed t*-tests). **e** Representative current responses from WT (top) or *Slc1a3*$^{P290R/+}$ (bottom) RGLs to puffs of 0.5 mM GABA for 5 s (holding potential of -70 mV). **f** Mean GABA uptake current amplitudes of WT and *Slc1a3*$^{P290R/+}$. Shown are individual responses to GABA applications (small symbols) and means of animals ($N = 8/12$, WT/*Slc1a3*.$^{P290R/+}$, $p = 0.021$, *two-tailed t*-test -Welch corrected)

to WT controls, by approximately 63% ($P \leq 0.001$; *two-way* ANOVA, Holm–Šidák post hoc tests; Fig. 2b). This deficit was reversed by pharmacological inhibition of the glial glutamate transporter EAAT1/GLAST with UCPH-101 [1], restoring tonic current amplitudes to WT levels ($p = 0.80$; Fig. 3b). Tonic inhibition declined with age in DG granule cells of WT animals, in line with previous reports [25], but this age-dependent reduction was absent in *Slc1a3*$^{P290R/+}$ mice, suggesting altered homeostatic regulation of GABA levels in the mutant genotype (Fig. 2b). Tonic GABAergic currents in layer 2/3 cortical pyramidal neurons of WT mice were approximately 42% smaller compared to DG neurons, but significantly reduced in *Slc1a3*$^{P290R/+}$ mice before the onset of seizures (P15-P20) ($p = 0.043$; *two-tailed t*-test; Fig. 2c).

Tonic GABAergic currents are predominantly mediated by δ subunit-containing $GABA_A$Rs [64], and we therefore analysed hippocampal and cortical tissue lysates for changes in δ subunit expression by western blotting. Hippocampal and cortical δ subunit levels did not differ between *Slc1a3*$^{P290R/+}$ and WT samples (Fig. 2d, Hippocampus: (d ‘), $p = 0.195^{P20}/0.888^{P40}$, Cortex: (d “), $p = 0.115$, *two-tailed t*-tests), suggesting that the observed reduction in tonic inhibition was not due to altered receptor abundance. Notably, only male mice were used for the analysis to avoid confounding effects related to δ subunit expression fluctuations during the ovarian cycle [43]. These findings point toward a decrease in ambient GABA levels, rather than receptor expression, as the

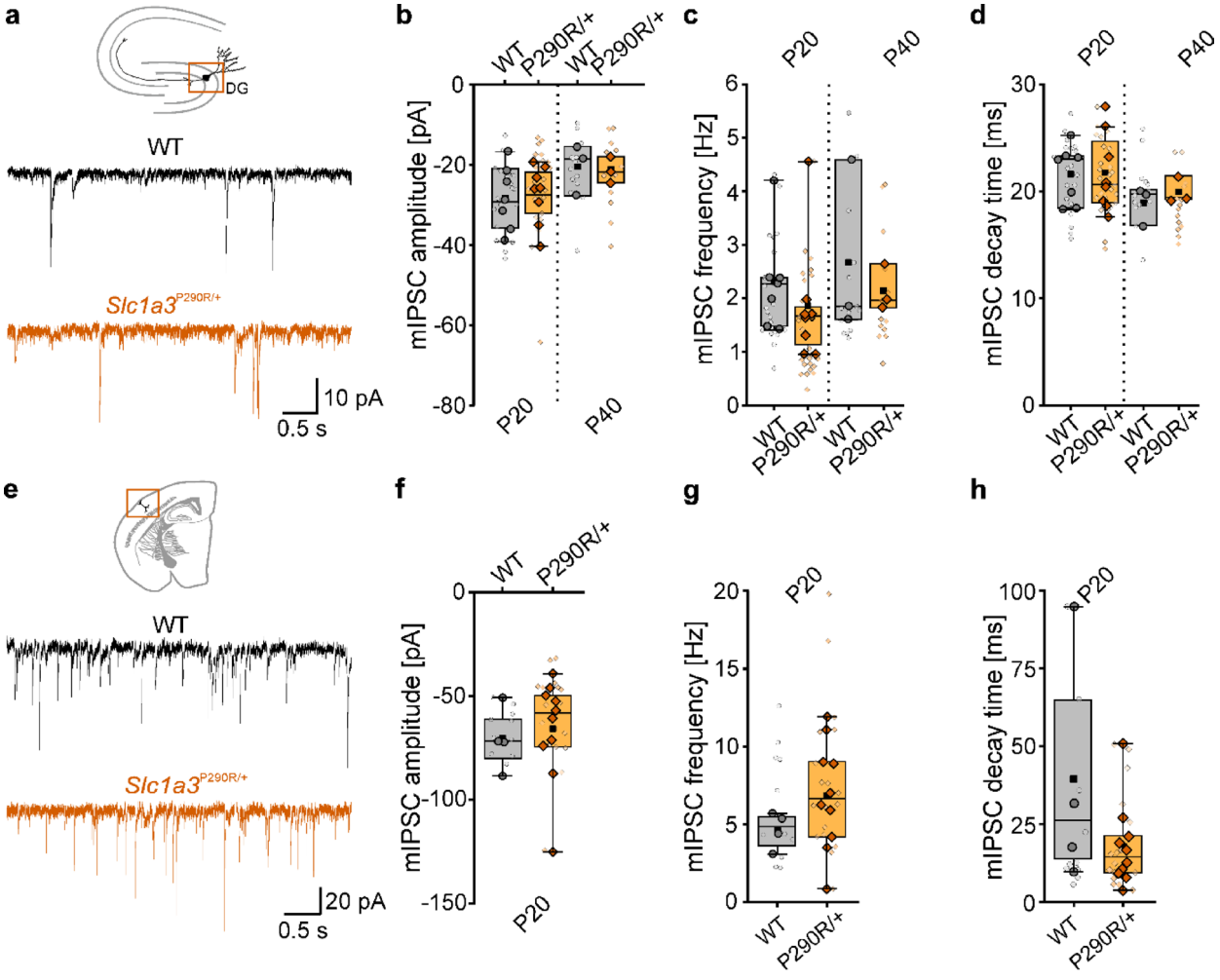

Fig. 3 Phasic GABAergic transmission is not altered in *Slc1a3*$^{P290R/+}$ mice. **a** Representative miniature inhibitory postsynaptic current (mIPSC) traces recorded from dentate gyrus (DG) granule cells of wildtype (WT) and *Slc1a3*$^{P290R/+}$ mice at P20. **b-d** Mean mIPSC amplitudes (I), frequencies (ν) and decay times (τ) recorded from DG granule cells at P20 (before seizure onset; $n = 19/26$ cells from $N = 7/8$ animals, $p = 0.82^{I}/0.42^{\nu}/0.95^{\tau}$, WT/*Slc1a3*$^{P290R+}$) and P40 (after seizure onset; $n = 14/13$, $N = 3/3$, WT/*Slc1a3*$^{P290R+}$, $p = 0.86^{I}/0.62^{\nu}/0.43^{\tau}$). **e** Representative mIPSC traces recorded from layer 2/3 (L2/3) pyramidal neurons of the somatosensory cortex from WT and *Slc1a3*$^{P290R/+}$ mice (before seizure onset). **f–h** Mean mIPSC amplitudes, frequencies and decay times recorded from L2/3 cortical pyramidal cells at P15-P20 (before seizure onset; $n = 11/18$, $N = 4/10$, WT/*Slc1a3*$^{P290R+}$, $p = 0.74^{I}/0.24^{\nu}/0.13^{\tau}$). Patch clamp data were analysed with *one-way* ANOVAs within ages and Holm–Šidák post hoc tests

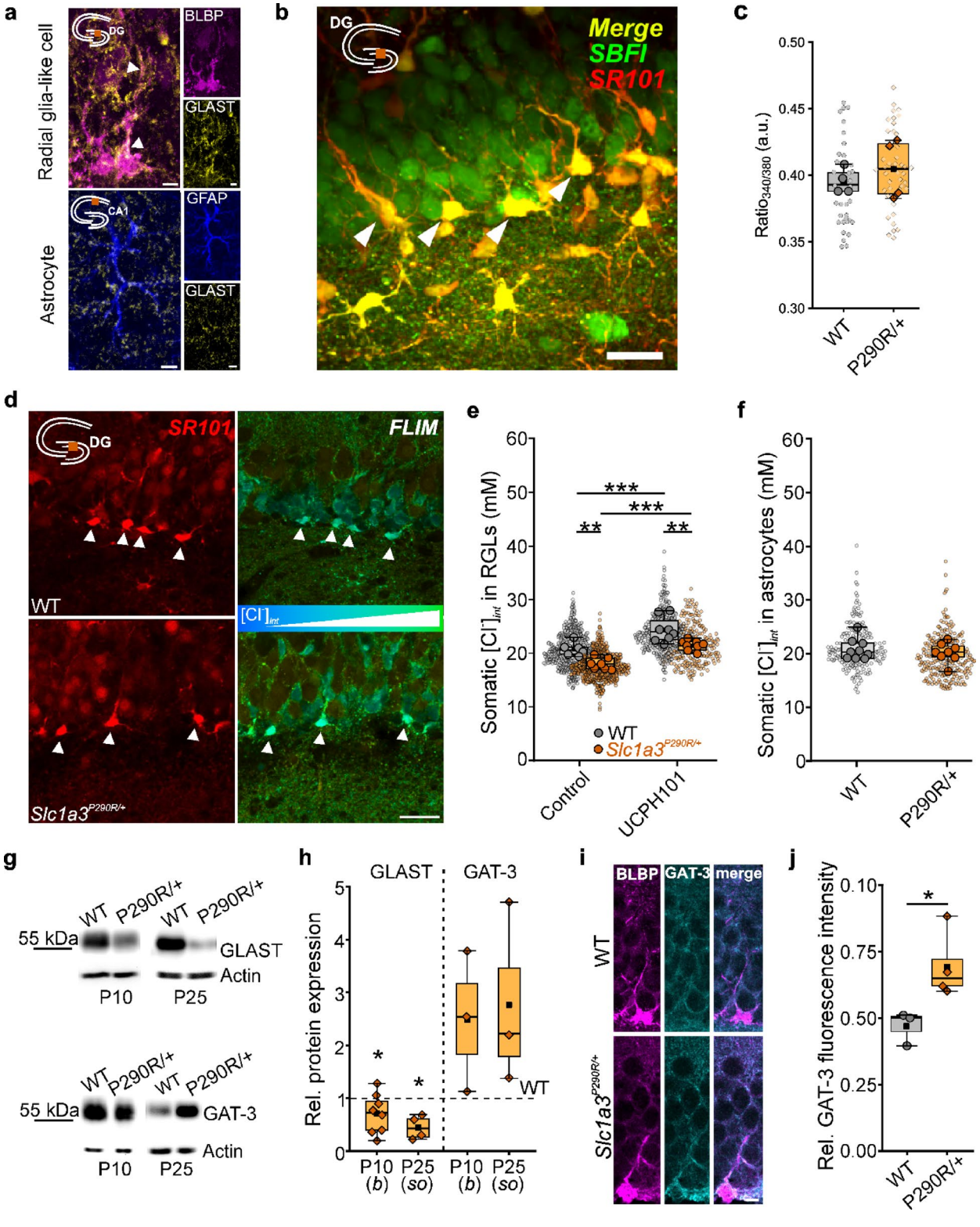

Fig. 4 (See legend on next page.)

(See figure on previous page.)

Fig. 4 Changes in intracellular ion concentrations in radial glia-like cells (RGLs) of *Slc1a3*$^{P290R/+}$ mice. **a** Confocal imaging of RGLs (DG) and astrocytes (CA1) confirm expression of EAAT1/GLAST (EAAT1/GLAST: yellow; BLBP—brain lipid binding protein (magenta); glial fibrillary acidic protein (GFAP): blue). EAAT1/GLAST-positive main processes of RGLs are indicated by arrowheads. Scale bar: 5 µm. **b** Multi-photon overview image showing a maximal projection of the Na^+ sensitive indicator SBFI (green) and the glia cell exclusive staining with sulforhodamine 101 (SR101, red). White triangles highlighting radial glia like cells. Scale bar: 20 µm. **c** Boxplots summarizing SFBI recordings from WT and *Slc1a3*$^{P290R/+}$ animals between P22 and P27 ($n = 34/40$, $N = 5/4$, WT/*Slc1a3*$^{P290R/+}$, $p = 0.09$). **d** Representative fluorescence lifetime imaging microscopy (FLIM) recordings in the hippocampal subgranular zone (P25). Arrowheads mark SR101-positive RGLs; color-coded scale indicates $[Cl^-]_{int}$. Scale bar: 25 µm. **e** Mean $[Cl^-]_{int}$ in RGLs from wildtype (WT) (grey circles) and *Slc1a3*$^{P290R/+}$ (orange circles) mice at P20–P30 ($n = 622/616$ (small circles) from $N = 6/7$ (big circles), WT/*Slc1a3*$^{P290R+}$, $p = 0.004$). Application of the EAAT1/GLAST-specific inhibitor UCPH-101 increased RGL $[Cl^-]_{int}$ in both genotypes ($n = 423/272$, $N = 8/7$, WT/*Slc1a3*$^{P290R/+}$, $p \leq 0.001 / \leq 0.001$, WT/*Slc1a3*$^{P290R+}$), although a significant difference between the genotypes remained ($p = 0.0012$, *two-way* ANOVA, Holm–Šidák post hoc tests). **f** Mean $[Cl^-]_{int}$ in CA1 astrocytes from individual WT (grey) and mutant (orange) mice at P20–P30 ($n = 206/277$, $N = 9/8$, WT/*Slc1a3*$^{P290R+}$, $p = 0.53$). Boxplots in (**e**) and (**f**) show distributions of $[Cl^-]_{int}$ from individual WT (grey) and *Slc1a3*$^{P290R/+}$ (orange) for animals (large circles, *N*) and single cells (small circles, *n*). **g** Western blot analysis of GLAST and GAT-3 expression in hippocampal tissue before seizure onset (*b*) at P10 ($N = 4/4$, $p = 0.0247^{GLAST}/0.07^{GAT-3}$) and during seizure onset (*so*) at P25 ($N = 3/4$, WT/*Slc1a3*$^{P290R+}$, $p = 0.02^{GLAST}/0.09^{GAT-3}$, *two-tailed t*-tests within age groups). **h** Quantification of western blot analyses in (**g**). **i** Representative confocal images of BLBP-positive (magenta) RGLs co-expressing GAT-3 (cyan; scale bar: 10 µm). **j** Mean GAT-3 fluorescence intensities normalised to BLBP signal at the single-cell level. Boxplots compare means (squares) and medians (lines) from individual animals ($N = 3/4$, WT/*Slc1a3*.$^{P290R+}$, $p = 0.043$, *two-tailed t*-test)

likely cause of diminished tonic inhibition in the DG and somatosensory cortex.

In the hippocampus, EAAT1/GLAST is expressed in astrocytes as well as in RGLs of the DG [4, 30]. RGLs are spatially associated with DG granule cells [46], suggesting a role in regulating the synaptic and extrasynaptic neurotransmitter environment of these neurons. Changes in GABA clearance by RGLs may thus contribute to the reduction of tonic inhibition in *Slc1a3*$^{P290R/+}$ mice. RGLs take up GABA via the Na^+-dependent GAT-3 transporter, and the electrogenic GABA uptake can be quantified by electrophysiological approaches [5, 33]. We evoked GAT-3-mediated currents by pressure GABA puffs in whole-cell patch clamp recordings from RGL cells at holding potentials of -70 mV (Fig. 2e). To isolate GAT-3 currents from other current components, $GABA_A$ and $GABA_B$ receptors were blocked with PTX (100 µM) and CGP55845 (1 µM), respectively [12, 51]. We found GAT-3 currents in mutant RGLs to be approximately twofold increased as compared to WT ($p = 0.021$, Fig. 2f, *two-tailed t*-test, Welch-corrected).

We next assessed phasic inhibition by recording $GABA_AR$-mediated miniature inhibitory postsynaptic currents (mIPSCs) in DG granule cells (Fig. 3a) and layer 2/3 cortical pyramidal neurons (Fig. 3e). The amplitude, frequency, and decay kinetics of mIPSCs did not differ between *Slc1a3*$^{P290R/+}$ mice and their WT littermates, indicating preserved synaptic GABAergic transmission in both hippocampal and cortical circuits during early postnatal development (Fig. 3b–d, f–h). Both, tonic and phasic inhibitory current amplitudes in CA1 pyramidal neurons remained unaffected at this developmental stage ($p = 0.67^{tonic}/0.39^{phasic}$, Supplementary Fig. 2). The regional specificity reinforces the DG as a key site of early tonic inhibitory dysfunction in this epilepsy model, but also suggests a potential, though less significant, contribution from the cortex to epileptogenesis. After seizure onset, both phasic and tonic GABAergic currents in DG granule cells were comparable between genotypes (Figs. 2b, 3b–d), suggesting a transient and developmentally specific deficit in inhibition. Our observations suggest that enhanced GAT-3 mediated GABA uptake reduce extrasynaptic GABA levels and thereby contribute to diminished tonic inhibition.

Intracellular $[Cl^-]$ is reduced in radial glia-like cells, but not in hippocampal astrocytes of *Slc1a3*$^{P290R/+}$ mice

EAAT1/GLAST is expressed in hippocampal RGLs and CA1 astrocytes (Fig. 4a). GABA transport into glial cells is driven by Na^+ and Cl^- gradients [41], and changes in EAAT1 function may modify glial $[Na^+]_{int}$—via coupled Na^+/H^+/glutamate: K^+ transport – as well as glial $[Cl^-]_{int}$ [18, 58] via EAAT anion channel function. Ratiometric measurements using the Na^+ indicator SBFI-AM [39] revealed no differences in $[Na^+]_{int}$ between WT and mutant RGLs (Fig. 4b, c; $p = 0.09$, $N = 8/7$ slices). Using fluorescence lifetime imaging microscopy (FLIM) and the Cl^--sensitive dye MQAE, we quantified $[Cl^-]_{int}$ in RGLs (Fig. 4d, e) and CA1 astrocytes (Fig. 4f) from P20–P30 mice of both sexes [18, 58]. RGLs from *Slc1a3*$^{P290R/+}$ mice displayed significantly reduced $[Cl^-]_{int}$ compared to WT RGLs (Fig. 4e; $20.8 \pm 1.0/18.0 \pm 0.8$ mM, ± *CI*, $N = 6/7$ mice, WT/*Slc1a3*$^{P290R/+}$; $p = 0.004$; *one-way* ANOVA, Holm–Šidák post hoc test). Incubation with the specific EAAT1/GLAST blocker UCPH-101 (20 µM) restored $[Cl^-]_{int}$ in mutant RGLs to levels close to those of untreated WT cells (Fig. 4e; $p = 0.471$, $N = 6/7$, WT/*Slc1a3*$^{P290R/+}$). In the presence of UCPH-101, $[Cl^-]_{int}$ was lower in *Slc1a3*$^{P290R/+}$ (Fig. 4e) than in WT RGLs (Fig. 4e; 24.4 ± 1.6 mM / 21.4 ± 0.7 mM, $p = 0.0012$, $N = 8/7$, WT/*Slc1a3*$^{P290R/+}$; *one-way* ANOVA, Holm–Šidák post hoc test), suggesting a compensatory upregulation of alternative Cl^--extruding mechanisms in RGLs of *Slc1a3*$^{P290R/+}$ animals [32]. In contrast, $[Cl^-]_{int}$ in CA1 astrocytes did not differ between genotypes under baseline conditions (Fig. 4f;

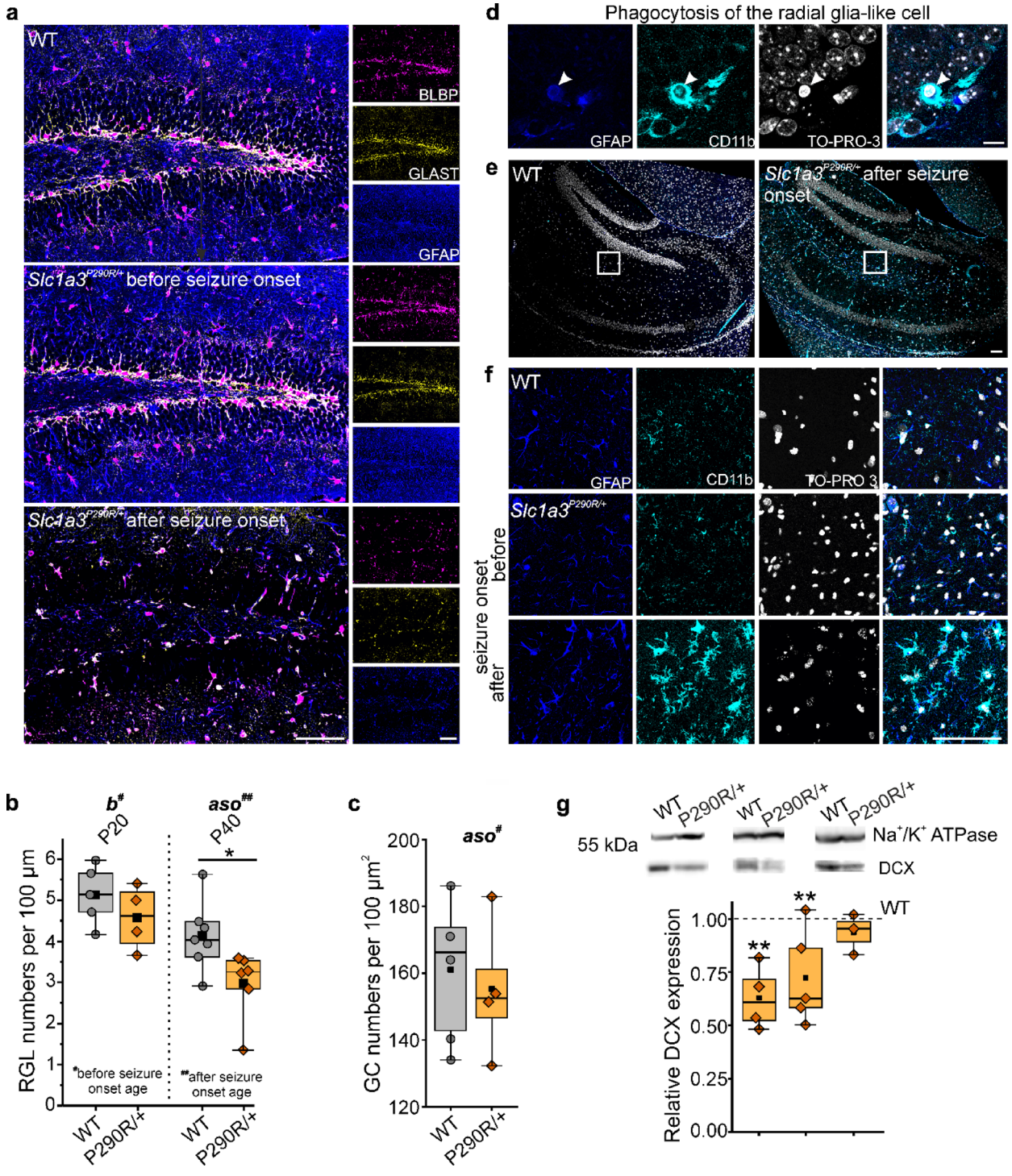

Fig. 5 (See legend on next page.)

20.8 ± 1.3/20.2 ± 1.3 mM, $N = 9/8$ mice, WT/*Slc1a3*$^{P290R/+}$; $p = 0.53$; *one-way* ANOVA, Holm–Šidák post hoc test).

Western blot analysis of hippocampal lysates showed a non-significant tendency for GAT-3 upregulation in *Slc1a3*$^{P290R/+}$ mice before (*b*, P10) and at the age of seizure onset (*so*, P25) (Fig. 4g, h; $p = 0.068^{b}/0.086^{so}$; *two-tailed t*-tests). EAAT1/GLAST protein levels were reduced in hippocampal lysates of heterozygous mice—by 29% in the second postnatal week and by 56% at seizure onset (Fig. 4h, i; $P10^{b}$: $p = 0.025$; $P25^{so}$: $p = 0.021$; *two-tailed t*-tests). Co-immunostaining for GAT-3 and BLBP confirmed their co-localisation in RGL somata and

(See figure on previous page.)

Fig. 5 Structural and cellular alterations in the hippocampus of adult *Slc1a3*$^{P290R/+}$ mice. **a** Representative confocal images of the dentate gyrus (DG) region from wildtype (WT) (P27, top) or *Slc1a3*$^{P290R/+}$ mice before (P20) and after (P40) age of seizure onset, immunolabeled for brain lipid binding protein (BLBP) (magenta), EAAT1/GLAST (yellow) and GFAP (blue). A marked reduction in radial glia-like cells (RGLs) is evident in mutants following seizure onset (middle: P23^{bfo}, bottom: P27^{aso}, scale bar: 100 µm). **b** RGL densities in WT and mutant animals at P20 and P40: P20^{bfo}, $N = 4/4$, WT/*Slc1a3*$^{P290R+}$, $p = 0.29$; P40^{aso}, $N = 7/7$; $p = 0.006$) **c** Comparison of granule cell (GC) numbers from WT and *Slc1a3*$^{P290R/+}$ mice at ages after seizure onsets (*aso*) shows no significant difference between genotypes ($p = 0.7$, $N = 5/4$, WT/*Slc1a3*$^{P290R+}$, *two-tailed t*-test). **d** Confocal images of the subgranular zone in a mutant DG (P27) depicting phagocytic events. Glial fibrillary acidic protein (GFAP)-positive (blue) astrocytes display condensed apoptotic nuclei (TOPRO-3, grey) surrounded by CD11b-positive (cyan) microglial processes. Scale bar: 10 µm. **e** Overview of hippocampal sections stained for GFAP and CD11b, with nuclear counterstain (TOPRO-3). **f** Higher magnification of the stratum lacunosum-moleculare reveals hypertrophic GFAP-positive astrocytic processes and increased microglial branching in mutants, consistent with reactive astrocytosis and microgliosis after seizures (P27; scale bars in (**d**) and (**e**): 100 µm). **g** Western blot analysis of doublecortin X (DCX) expression in hippocampal tissue at P10 ($N = 4/4$), P20 ($N = 5/5$) and P40 ($N = 3/3$, WT/*Slc1a3*$^{P290R+}$). Na^+/K^+-ATPase served as loading control. The graph shows DCX expression in mutants relative to WT levels (dashed line); $p = 0.0025^{P10}/0.0072^{P20}/0.1741^{P40}$)

their vertically oriented processes extending into the DG granule cell layer (Fig. 4i). Direct quantification of fluorescence intensities by fluorescence microscopy (Fig. 4i, j) demonstrated a significantly increased GAT-3 signal within RGLs of P25 *Slc1a3*$^{P290R/+}$ mice compared to WT controls ($N = 3/4$, WT/*Slc1a3*$^{P290R/+}$, $p = 0.043$, *two-tailed t*-test).

We conclude that the P290R-associated gain-of-function in EAAT1/GLAST anion channel activity reduces the $[Cl^-]_{int}$ in hippocampal RGLs and simultaneously increases GAT-3 expression in RGLs. The resulting increase in the driving force for GAT-3-mediated GABA uptake, together with elevated RGL-specific GAT-3 expression, may reduce extracellular GABA levels and consequently tonic inhibition in the DG of *Slc1a3*$^{P290R/+}$ mice.

Hippocampal RGLs are reduced in *Slc1a3*$^{P290R/+}$ mice during the postictal phase

In the cerebellum of *Slc1a3*$^{P290R/+}$ animals, apoptosis of Bergmann glial cells is triggered by the aberrantly increased anion channel activity caused by the P290R variant [37]. To test whether a similar glial pathology occurs in the hippocampus of *Slc1a3*$^{P290R/+}$ mice, we quantified RGLs in the DG from WT and mutant mice of both sexes at stages preceding and following seizure onset using immunohistochemistry. Confocal imaging of hippocampal section immunolabeled for the glial markers BLBP, GFAP, and GLAST revealed comparable RGL densities in WT and mutant animals in the subgranular zone of the DG prior to seizure onset (P12-15; Fig. 5a, b; $p = 0.3$, *two-tailed t*-test). In contrast, a significant reduction in RGL density was observed in *Slc1a3*$^{P290R/+}$ mice older than P40 (Fig. 5a, b; $p = 0.021$, *two-tailed t*-test). The overall density of granule cells remained unchanged in mutant mice after epilepsy onset (Fig. 5c; $p = 0.7$, *two-tailed t*-test). At P27, we detected CD11b-positive microglia containing GFAP-positive cell fragments in the subgranular zone of *Slc1a3*$^{P290R/+}$ mice, consistent with active phagocytosis of astroglial cells (Fig. 5d). This was accompanied by pronounced hippocampal astrocytosis, characterized by hypertrophy of astrocytic somata and processes, and microgliosis, indicated by increased CD11b expression (Fig. 5e, f).

To assess whether impaired RGL survival affects neurogenesis, we examined expression of doublecortin X (DCX), a marker of immature granule cells, by western blot analysis. DCX protein levels were reduced in *Slc1a3*$^{P290R/+}$ hippocampi prior to seizure onset but returned to control levels at P40 (Fig. 5g; $p = 0.0025^{P10}/0.0072^{P20}/0.174^{P40}$; *two-tailed t*-tests), indicating a transient impairment of neurogenesis during early postnatal development. Since RGLs serve as neural progenitors that give rise to granule cells in the DG, their loss is likely to directly impact the generation of new neurons. Taken together, these observations indicate that expression of the P290R EAAT1/GLAST mutant in RGLs disrupts hippocampal neurogenesis through a mechanism independent of seizure activity.

Slc1a3$^{P290R/+}$ mice show an abnormal reactive astrogliosis in the hippocampus

Hippocampal formations from *Slc1a3*$^{P290R/+}$ mice displayed a neuroanatomically regular architecture (Fig. 6), without significant neuronal rarefication, particularly no segmental loss of neurons at different time points after birth, including P5, P10 and P35. The density of DG granule cells appeared unaltered at all examined ages, and granule cell dispersion was absent. At P5, the pyramidal band and DG showed no relevant infiltration by reactive astrocytes, whereas by P35, astroglial cell elements were frequently found adjacent to neuronal elements, as revealed by GFAP immunohistochemistry (Fig. 6). This cellular reactive astrogliosis affecting the hippocampal formation emerged at P10 and was neuropathologically most pronounced at P35. Age-matched WT animals do not show astrogliosis (Fig. 6). More chronic fibrillary astrogliotic changes were not observed. The changes observed in *Slc1a3*$^{P290R/+}$ resemble the 'gliosis only' phenotype of temporal lobe epilepsy (TLE) [23, 24], while hippocampal sclerosis, as the most frequently pathological change observed in TLE [3], was absent.

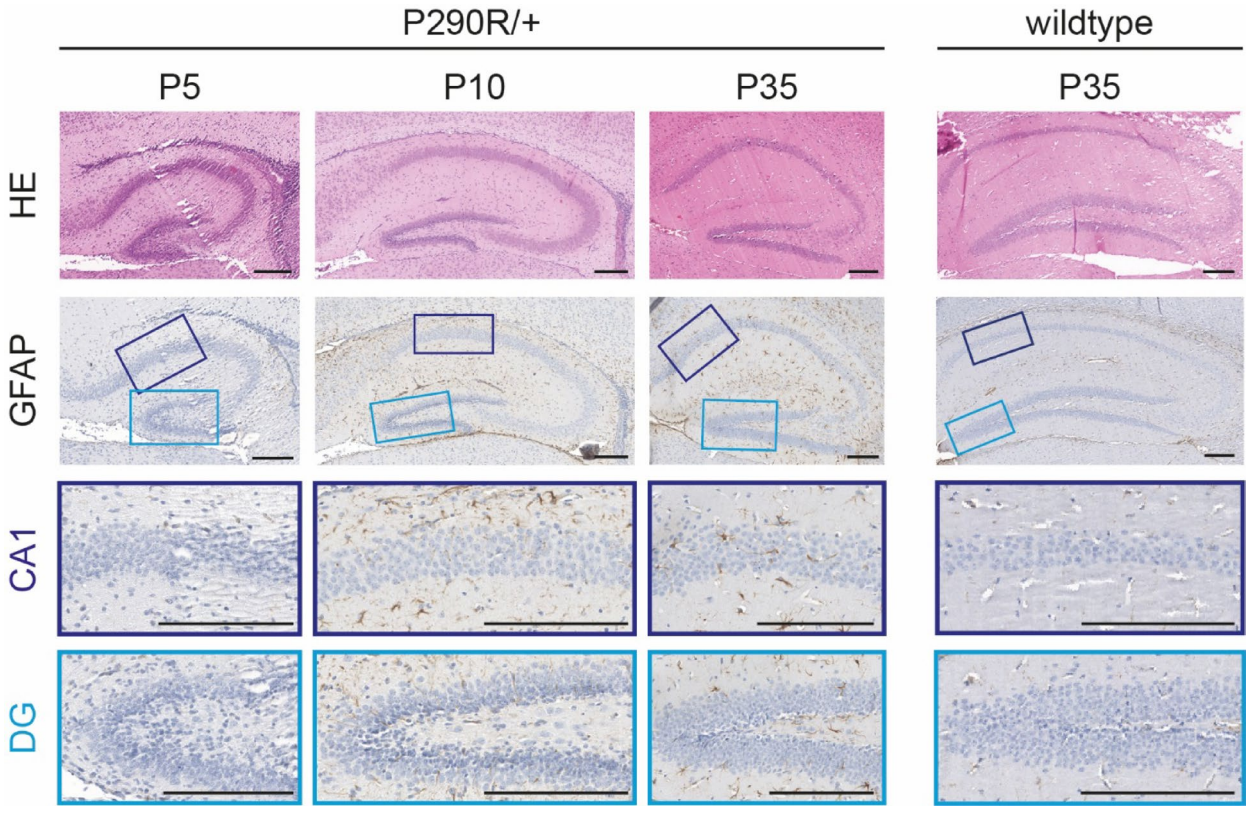

Fig. 6 *Slc1a3*$^{P290R/+}$ hippocampi show a *´gliosis only´* phenotype. Hippocampal formations of brains isolated from *Slc1a3*$^{P290R/+}$ at days 5 and 10 after birth (P5/10, *far ahead from paroxysmal period*) and 35 (P35, *within paroxysmal period*) and WT mice (P35) stained with hematoxylin and eosin (HE, upper row) and subjected to immunohistochemistry with antibodies against glial fibrillary acidic protein (GFAP, second row). Below, higher power magnifications of CA1 (from purple squares in 'GFAP') and dentate gyrus (DG; from light blue squares in 'GFAP'; all scale-bars: 200 µm)

Excitatory transmission is unaltered prior to seizure onset of *Slc1a3*$^{P290R/+}$

Ionotropic glutamate receptors, including amino-3-hydroxy-5-methyl-4-isoxazolepropionic acid receptors (AMPARs) and N-methyl-D-aspartate ionotropic glutamate receptors (NMDARs), play distinct roles in epileptiform activity, with AMPARs being particularly important for the initiation of epileptic discharges [5]. To evaluate AMPAR-mediated synaptic transmission in the hippocampus, we recorded miniature excitatory postsynaptic currents (mEPSCs) in DG granule cells and CA1 pyramidal neurons from both juvenile (P20) and adult (P40) *Slc1a3*$^{P290R/+}$ and WT animals of both sexes (Fig. 7a, e). Recordings at P20 revealed similar mEPSC amplitudes, frequencies, and decay kinetics in both genotypes and both tested regions (Fig. 7b–d, f–h). In CA1 neurons, mEPSC amplitudes were slightly increased in P40 *Slc1a3*$^{P290R/+}$ mice compared to WT controls ($p = 0.023$; Fig. 7f), whereas the frequency and decay times remained unchanged (Fig. 7g–h). In contrast, mEPSC characteristics in DG granule cells remained unaltered between *Slc1a3*$^{P290R/+}$ and WT mice at P40 (Fig. 7b–d). AMPAR-mediated mEPSCs in layer 2/3 pyramidal neurons of the somatosensory cortex at a juvenile, pre-seizure stage (P15–20) (Fig. 7i) neither differed in mEPSC amplitudes, frequencies nor decay times between juvenile heterozygous and WT mice (Fig. 7j–l).

To test whether the increased mEPSC amplitude in CA1 pyramidal neurons after seizure onset is associated with altered neurotransmitter receptor expression, we used quantitative autoradiography to measure AMPAR, $GABA_BR$, and metabotropic glutamate 2/3 receptor (mGlu2/3R) densities in WT and mutant mice from both sexes [66]. We found increased AMPAR densities in the caudatum putamen, motor and sensory cortices, and the hippocampal region of *Slc1a3*$^{P290R/+}$ mice at P45 (Fig. 8a–c). The AMPAR density was elevated in the CA1 region, consistent with the increased mEPSC amplitude detected in CA1 pyramidal cells (Fig. 7f, 8c). In contrast, the AMPAR density was reduced in the cerebellum of *Slc1a3*$^{P290R/+}$ animals (Fig. 8d), likely reflecting the progressive glial and neuronal degeneration in this brain region [37]. The cerebellar downregulation was also observed for other tested receptors. Densities of all other tested receptors were unaffected in the cerebrum of adult *Slc1a3*$^{P290R/+}$ mice, except for mGlu2/3 receptors, which were decreased by approximately 37% in the CA1 region (data not shown as figure, for raw data refer to raw data

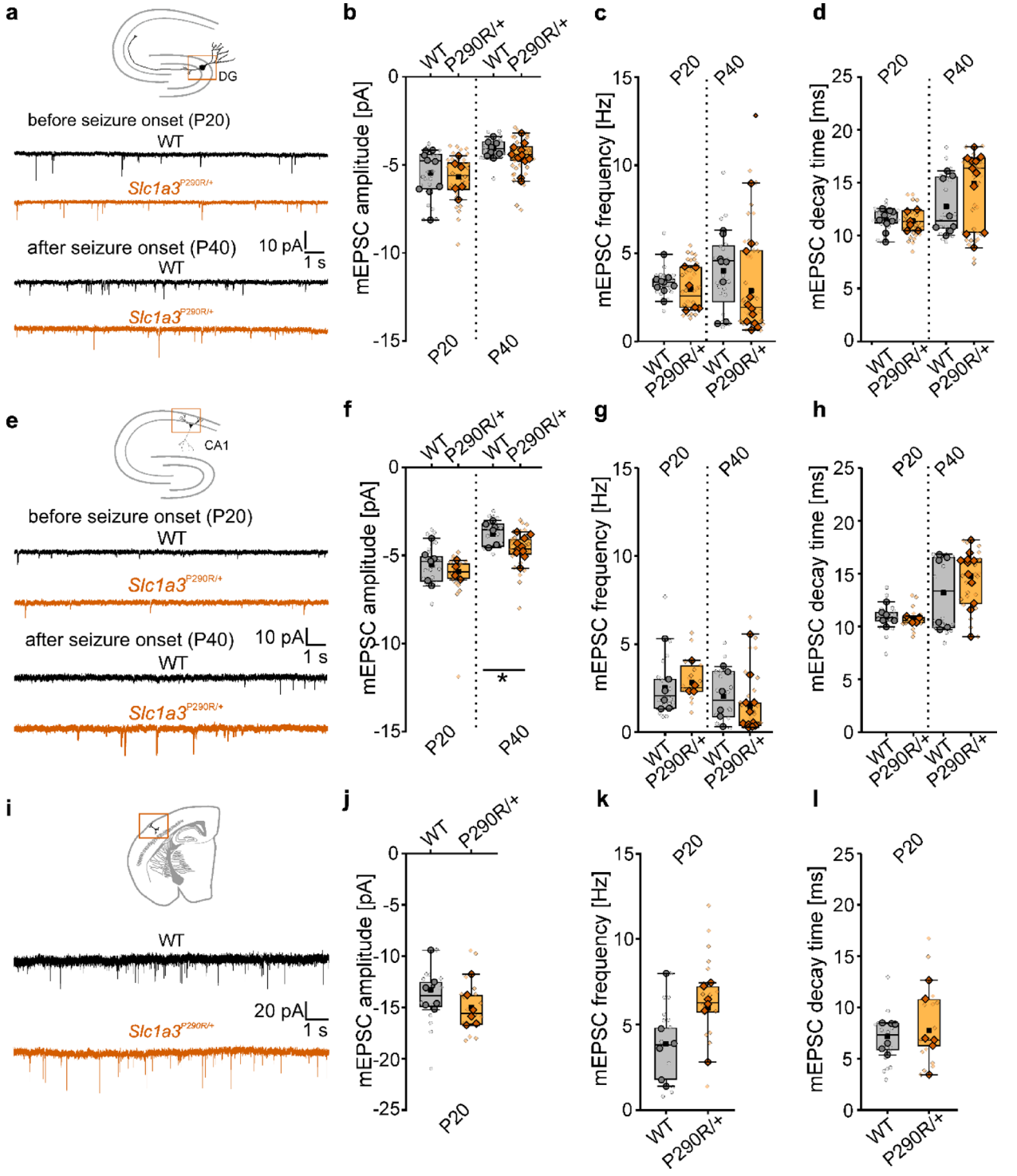

Fig. 7 Excitatory transmission is unaltered before seizure onset in *Slc1a3*$^{P290R/+}$ mice. **a** Representative miniature inhibitory postsynaptic current (mEPSC) traces recorded from dentate gyrus (DG) granule cells at P20 (before seizure onset) and P40 (after seizure onset). **b**–**d** mEPSC amplitudes (I), frequencies (ν) and decay times (τ) of mEPSCs in DG granule cells at P20 ($n = 17/28^{I,\nu}$,29^{τ} WT/*Slc1a3*$^{P290R/+}$ cells, $N = 10/6$ mice, $p = 0.44^{I}/0.32^{\nu}/0.9^{\tau}$) and P40 ($n = 20/33$, $N = 8/11$, $p = 0.21^{I}/0.33^{\nu}/0.14^{\tau}$). **e** Representative mEPSCs recorded from CA1 pyramidal neurons at P40. **f**–**h** Amplitudes, frequencies and decay times of mEPSCs in CA1 pyramidal neurons at P20 ($n = 18/14$, $N = 7/4$, WT/*Slc1a3*$^{P290R/+}$, $p = 0.43^{I}/0.72^{\nu}/0.46^{\tau}$) and P40 ($n = 16/25$, $N = 6/10^{I},11^{\nu,\tau}$, $p = 0.02^{I}/0.48^{\nu}/0.36^{\tau}$). **i** Representative mEPSC traces recorded from layer 2/3 (L2/3) pyramidal neurons of the somatosensory cortex at P15-P20. **j**–**l** Amplitudes, frequencies and decay times of mEPSCs in L2/3 pyramidal cells at P15-P20 ($n = 14/15$, $N = 6/6$, $p = 0.17^{I}/0.12^{\nu}/0.65^{\tau}$). Patch-clamp data were analysed using *one-way* ANOVAs within ages and Holm–Šidák post hoc tests

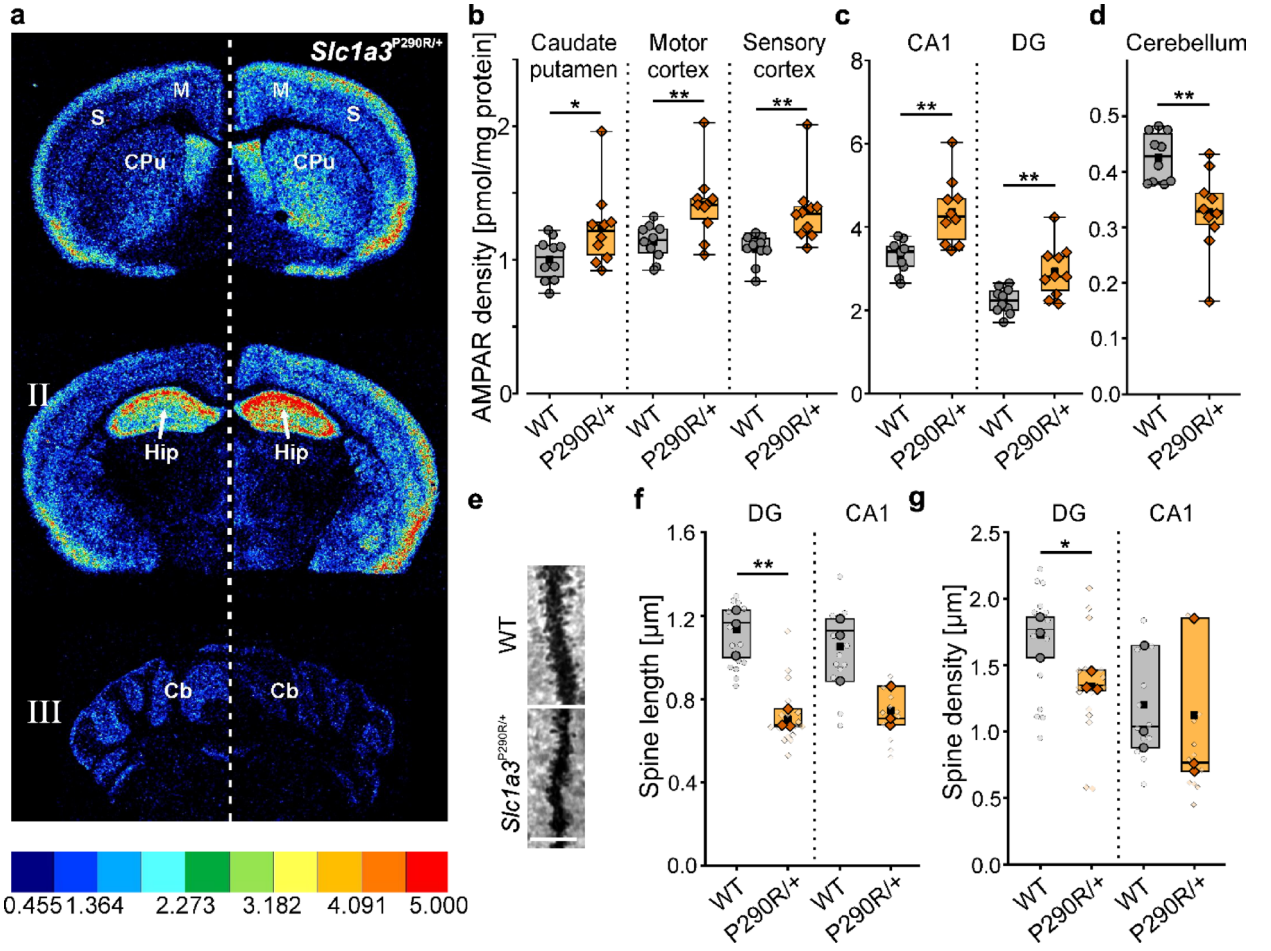

Fig. 8 Hippocampal AMPAR densities and neuronal spine density are altered in adult *Slc1a3*$^{P290R/+}$ mice. **a** Contrast-enhanced color-coded (*inset*) AMPAR densities in the brain of wild-type (*left*) and *Slc1a3*$^{P290R/+}$ mice (*right*). Three cutting planes (I–III) show I, the caudate putamen (Cpu), the motor (M) and sensory (S), cortex; II, the hippocampus (Hip); and III, the cerebellum (Cb). The assigned color scale represents equally spaced density ranges in pmol/mg protein. Scale bar: 1000 µm **b**–**d** AMPAR densities from the indicated brain regions (Cpu: $p = 0.042^{Cpu}/0.0086^{M}/0.0046^{S}/0.0013^{CA1}/0.0015^{CA2/3}/0.0056^{DG}/0.0021^{Cb}$, *two-tailed t*-tests, $N = 10/10$ animals, WT/*Slc1a3*$^{P290R/+}$). **e** Representative Golgi–Cox-stained secondary and tertiary dendrites of WT and *Slc1a3*$^{P290R/+}$ granule cells (> P70, scale bar: 5 µm). **f** Mean spine lengths in DG and CA1 neurons (DG: 1.13 ± 0.12 /0.72 ± 0.15 µm; CA1: 0.95 ± 0.2/0.75 ± 0.09 µm, means ± SD, WT/*Slc1a3*$^{P290R+}$, $p = 0.004^{DG}/0.16^{CA1}$, *two-tailed t*-tests). **g** Mean spine density measured in WT and mutant animals in DG and CA1 neurons (DG: 1.73 ± 0.18/1.37 ± 0.07 spines/µm; CA1: 1.20 ± 0.44/1.12 ± 0.7 spines/µm, $p = 0.045^{DG}/0.884^{CA1}$, WT/*Slc1a3*$^{P290R+}$, *two-tailed t*-tests). (**f**) and (**g**) present data for dendritic spines in 10 µm dendritic segments of DG granule cells and CA1 pyramidal cells (large symbols: $N = 3/3$, WT/*Slc1a3*.$^{P290R+}$, small symbols: means from individual slices)

file at https://github.com/peterkovermann/episodic_ataxia_6_II/). We conclude that AMPAR-mediated excitatory synaptic transmission in the hippocampus and neocortex is largely unaltered prior to seizure onset in *Slc1a3*$^{P290R/+}$ mice (Fig. 7), suggesting that glutamatergic signalling is not a driving factor in epileptogenesis.

To identify possible activity-dependent structural adaptations that may dampen hippocampal excitability and restrict epileptic activity, we analysed dendritic spine morphology in Golgi-Cox-stained DG granule cells and CA1 pyramidal cells from *Slc1a3*$^{P290R/+}$ mice after the peak-seizure period. Spine lengths were significantly reduced in secondary and tertiary dendrites of DG granule cells, but not in CA1 pyramidal neurons (Fig. 8e-f; $p = 0.004/0.16$, *two-tailed t*-tests). Additionally, spine density was selectively decreased in DG neurons (Fig. 8g; $p = 0.035$, *two-tailed t*-test). These structural alterations, including spine retraction, may reflect a compensatory form of synaptic pruning aimed at restraining network hyperexcitability in the epileptic hippocampus.

Discussion

We here investigated the cellular pathophysiology of a severe form of episodic ataxia type 6 associated with the P290R variant in the human *SLC1A3* gene [28] using the *Slc1a3*$^{P290R/+}$ knock-in mouse model that recapitulates key features of the human phenotype [37]. *Slc1a3*$^{P290R/+}$ animals exhibit a pronounced epileptic phenotype, particularly during a critical time window in early postnatal development (Fig. 1). Video-EEG recordings revealed

epileptic seizures and status epileptici at juvenile and later stages with increased seizure severity and high seizure-associated mortality, in juvenile mice (Fig. 1). Histological analysis revealed a pronounced astrogliosis in the hippocampus (Fig. 6), whereas other brain areas, including the cortex, showed no comparable gliotic response (data not shown). Regionally confined astrogliosis is a well-established marker of chronic neuronal hyperexcitability and is frequently observed at epileptogenic foci, particularly in hippocampal and limbic epilepsies [54]. The presence of hippocampal gliosis supports the hippocampal formation, rather than the neocortex, as the origin of seizure generation in *Slc1a3*$^{P290R/+}$ mice. In acute slices from mice, we did not detect any differences in the amplitude, frequency or decay kinetics of AMPA receptor-mediated mEPSCs in CA1 pyramidal neurons, DG granule cells or layer 2/3 cortical pyramidal neurons between WT and *Slc1a3*$^{P290R/+}$ animals at P20 (Fig. 7), indicating intact excitatory synaptic transmission at this developmental stage. Likewise, phasic GABAergic inhibitory transmission in DG granule cells and layer 2/3 cortical pyramidal neurons remains unaltered (Fig. 3). However, tonic GABAergic currents were markedly reduced in DG granule cells (Fig. 2), and only slightly attenuated in layer 2/3 cortical pyramidal neurons. Since EAAT1/GLAST is exclusively expressed in glial cells and not in neurons [31, 50], with a high expression in DG RGLs [15], a direct impact on DG granule cell excitability is not expected. Taken together, these findings indicate that glutamate transporter dysfunction contributes to the observed epilepsy in *Slc1a3*$^{P290R/+}$ mice by impairing tonic inhibition in the hippocampus, without significantly affecting glutamatergic synaptic transmission.

The DG plays a key role in regulating hippocampal excitability, and tonic GABAergic inhibition of granule cells is particularly important for modulating hippocampal network activity [10]. Disruption of tonic GABAergic inhibition is a well-established mechanism in epileptogenesis. Tonic GABAergic currents are mediated by $GABA_A$Rs containing δ subunits, which confer high sensitivity to ambient GABA and are typically located extrasynaptically [21]. Deletion of the δ subunit in mice leads to spontaneous seizures [52, 55], and variants that impair either the open probability or membrane trafficking of $GABA_A$Rs are associated with human epilepsy syndromes [22]. Moreover, δ subunit abundance varies across the ovarian cycle and correlates with fluctuations in seizure susceptibility, further highlighting the critical role of tonic inhibition in modulating network excitability [43].

In *Slc1a3*$^{P290R/+}$ DG granule cells, we observed reduced GABAergic tonic inhibition despite unchanged $GABA_A$R δ subunit expression levels (Fig. 2). These findings indicate that the attenuation of tonic inhibition is not due to altered receptor availability, but is likely driven by decreased ambient GABA levels in the microenvironment of granule cells. Decreased ambient GABA levels were associated with enhanced GABA uptake by mutant RGLs (Fig. 2e, f). GABA transporters (GATs) are driven by the electrochemical gradients of Na^+ and Cl^- [41], and we detected diminished $[Cl^-]_{int}$ in RGLs from *Slc1a3*$^{P290R/+}$ mice, which will increase the driving force for glial GABA uptake. Application of the EAAT1/GLAST-specific inhibitor UCPH-101 restored both tonic GABAergic inhibition (Fig. 2b) and $[Cl^-]_{int}$ in RGLs to WT levels (Fig. 4e), indicating a mechanistic link between these alterations and P290R EAAT1/GLAST gain-of-anion channel function. RGL $[Cl^-]_{int}$ was only reduced by about 15% as compared to WT values, a rather small change to account for the observed threefold increase of GAT-3 currents. However, we can only determine $[Cl^-]_{int}$ in the RGL soma, so that larger differences appear possible in glial extensions close to extrasynaptic localizations of granule cells. Moreover, we observed increased GAT-3 expression levels in young animals (Fig. 4g–j). $[Na^+]_{int}$ were not different between WT and mutant RGLs (Fig. 4b, c). It is tempting to speculate that enhanced GAT-3-mediated Na^+ inward transport in microdomains near granule cells could locally stimulate Ca^{2+} uptake via increased Na^+/Ca^{2+} exchange [52], which may promote GAT-3 upregulation [53]. These mechanisms could further reinforce GABA clearance from the extracellular space, thereby exacerbating the deficit in tonic inhibition.

We observed astrocytic and microglial activation in *Slc1a3*$^{P290R/+}$ animals (Fig. 5a–f), which may result from seizures [16, 61, 68] and may further exacerbate epileptic activity. After the fifth postnatal week, increased amplitudes of AMPAR-mediated mEPSCs were recorded in CA1 pyramidal cells (Fig. 7), and autoradiography experiments revealed increased AMPAR densities in the hippocampus of *Slc1a3*$^{P290R/+}$ animals (Fig. 8). The release of tumor necrosis factor alpha (TNF-α) by activated microglia, in conjunction with astrocytes [44], has been shown to enhance synaptic AMPAR number [47]. Moreover, epileptic discharges may directly potentiate AMPAR-mediated synaptic transmission in hippocampal neurons [14, 29], leading to excessive glutamatergic excitation and thus epileptic synchronisation. EEG recordings in *Slc1a3*$^{P290R/+}$ animals during the post-peak phase revealed persistent seizures and status epileptici, albeit with notably reduced severity and frequency. Interestingly, in some older animals, seizures were absent during the recording period. At this later stage, spine density in the DG was reduced, and dendritic spines in both DG and CA1 showed signs of retraction (Fig. 8f, g). Seizure activity may have led to activity-dependent elimination of synaptic connections at later time points, potentially

serving a protective role for hippocampal neurons in these animals [44, 47].

Whereas *Slc1a3*$^{P290R/+}$ Bergmann glia undergo apoptosis triggered by cell shrinkage at the onset of glutamatergic synaptic transmission [37], we observed only a modest reduction in the number of hippocampal RGLs (Fig. 5b). Apoptotic events in the hippocampal subgranular zone of *Slc1a3*$^{P290R/+}$ mice (Fig. 5d), along with downregulation of DCX (Fig. 5g), a marker of immature neurons, suggest that RGLs undergo apoptosis, but do not prematurely differentiate, thus preventing depletion of the RGL pool [17]. These findings imply that RGLs are less prone to apoptosis compared to Bergmann glia. A potential explanation for the differential responses between the two cell types may lie in the lower $[Cl^-]_{int}$ in RGLs, as opposed to Bergmann glial cells [18, 58].

Our results suggest that impaired tonic GABAergic inhibition in hippocampal granule cells, resulting from the dysfunction of the EAAT1/GLAST-associated anion channel, triggers the epileptic phenotype. The increased Cl^- efflux through the mutant EAAT1/GLAST leads to a reduction in $[Cl^-]_{int}$ in RGLs, facilitating GABA uptake via glial GAT-3. This depletion of ambient GABA around DG granule cells diminishes tonic GABAergic currents, which in turn induces hyperexcitability in the DG and contributes to the onset of epilepsy. Enhanced AMPAR-mediated synaptic transmission does not trigger but may contribute to the maintenance of epileptic discharges and facilitate prolonged seizures in older animals. We speculate that repetitive epileptic activity contributes to RGL loss, diminishes spine density and triggers dendritic spine retraction in principal hippocampal neurons, potentially helping to limit seizure frequency and severity at later stages (Fig. 1).

In recent years, an increasing number of neurological conditions has been linked to variants in *SLC1A2* or *SLC1A3*. Contrary to earlier assumptions, not the impairment of glutamate transport, but rather changes in EAAT1/2 anion channel function seem to trigger the disease [7, 34, 36, 37, 63, 65]. In certain cases of epileptic encephalopathies, *SLC1A2* mutations impair the selectivity of EAAT2 anion channels, resulting in glutamate conduction and presynaptic glutamate release [34, 36]. However, most pathogenic *SLC1A2* or *SLC1A3* variants leave anion channel selectivity intact and solely enhance anion channel activity [7, 34].

We, here link gain-of-anion channel function of P290R EAAT1 to increased GABA uptake and impaired tonic GABAergic inhibition as basis of hippocampal hyperexcitability. Inhibition of EAAT1/GLAST with the specific EAAT1 inhibitor UCPH-101 [1] restores the impaired tonic inhibition to WT levels (Fig. 2b), thus identifying selective EAAT1-block as promising therapeutic approach for *SLC1A3*-associated episodic ataxia. We hypothesize that GABAergic and glutamatergic neurotransmitter systems are functionally linked via the two EAAT transport functions, i.e. secondary-active glutamate transport and anion channel function [6, 19, 35, 42, 58]. Glutamate release from synapses activates EAAT1 anion channels, which reduce glial $[Cl^-]_{int}$ and subsequently enhance GABA uptake, leading to decreased tonic $GABA_AR$-mediated inhibition. This mechanism may contribute to adjusting the balance between excitatory and inhibitory synaptic transmission under physiological conditions. The severe epileptic phenotype in *Slc1a3*$^{P290R/+}$ mice represents a pathophysiological consequence of disrupted interaction between glutamatergic and GABAergic signalling arising from glial EAAT1/GLAST dysfunction.

Supplementary Information

The online version contains supplementary material available at https://doi.org/10.1186/s40478-026-02399-4.

Supplementary Material 1

Supplementary Material 2

Acknowledgements

We acknowledge the animal facility of the Forschungszentrum Jülich GmbH and the Transgenic Core Facility, a core facility of the Interdisciplinary Center for Clinical Research (IZKF) Aachen within the Faculty of Medicine at RWTH Aachen University. Furthermore, we thank Christoph Aretzweiler, Marcel Böttcher, Tanja Mertens, Ana Fulgencio Maisch, Heidi Löffler, Kameraj Myvledin, Claudia Roderigo, Simone Durry and Hang Lyu for their excellent technical support in performing various experimental procedures, animal care, and genotyping. We are also grateful to Nikola Kornadt-Beck for assistance with regulatory aspects of animal breeding, and to Andrei Kostritskii and Jennifer Cremer for valuable discussions.

Author contributions

Y.K., D.B-M., T.G., J.M., C.R., A.B., U.H., Ch.F and P.K. designed the research; Y.K., D.B-M., M.E., J.M., J.B., S.Be, S.Bl, and P.K. performed data aquisition and analysis. Y.K., D.B-M., J.B., J.M., A.B., U.H., Ch.F. and P.K. drafted the figures and the manuscript.

Funding

Open Access funding enabled and organized by Projekt DEAL. The project was supported from the Federal Ministry of Education and Research (E-RARE network Treat-ION: 01GM1907C to Ch.F. and 01GM1907G to U.H.; Project SynGluCross to C.R.R.) and the German Research Foundation (FOR 2795; FA 301/13–1 to Ch.F.; Project #461542557, RO 2327/13–2,14–2 to C.R.R.).

Data availability

All data supporting this study are publicly available on GitHub at the following URL: https://github.com/peterkovermann/episodic_ataxia_6_II/

Declarations

Ethics approval and consent to participate

All animal procedures were performed in accordance with the Animal Research guidelines (ARRIVE): Reporting of In Vitro and In Vivo experiments was approved by the appropriate animal care and use committees [LANUV (State Agency for Nature, Environment and Consumer Protection) of North Rhine-Westphalia (reference numbers: 84-02.04.2014.A334, 81-04.04.2020.A441), Regierungspräsidium Tübingen of Baden-Württemberg (reference number: N18/20G)]. Subsets of the data presented in this manuscript have been previously included in the doctoral theses from the two first authors YK and DBM.

Consent for publication
Not applicable.

Competing interests
The authors declare no competing interests.

Author details
[1]Institute of Biological Information Processing, Molekular- und Zellphysiologie (IBI-1), Forschungszentrum Jülich, 52428 Jülich, Germany
[2]Department of Neurology and Epileptology, Hertie Institute for Clinical Brain Research, University of Tübingen, 72076 Tübingen, Germany
[3]Institute of Neurobiology, Heinrich-Heine-Universität Düsseldorf, 40225 Düsseldorf, Germany
[4]Institute for Cellular Neurosciences II, Universitätsklinikum Bonn, 53127 Bonn, Germany
[5]Institute of Neuroscience and Medicine, Strukturelle und funktionelle Organisation des Gehirns (INM-1), Forschungszentrum Jülich GmbH, 52428 Jülich, Germany
[6]Present address: MSH Medical School Hamburg, 20457 Hamburg, Germany

Received: 21 May 2026 / Accepted: 31 July 2026
Published online: 04 August 2026

References

1. Abrahamsen B, Schneider N, Erichsen MN, Huynh TH, Fahlke C, Bunch L, Jensen AA (2013) Allosteric modulation of an excitatory amino acid transporter: the subtype-selective inhibitor UCPH-101 exerts sustained inhibition of EAAT1 through an intramonomeric site in the trimerization domain. J Neurosci 33:1068–1087. https://doi.org/10.1523/JNEUROSCI.3396-12.2013
2. Avanzini G, Franceschetti S (2003) Cellular biology of epileptogenesis. Lancet Neurol 2:33–42. https://doi.org/10.1016/s1474-4422(03)00265-5
3. Blumcke I, Thom M, Aronica E, Armstrong DD, Bartolomei F, Bernasconi A, Bernasconi N, Bien CG, Cendes F, Coras R et al (2013) International consensus classification of hippocampal sclerosis in temporal lobe epilepsy: a Task Force report from the ILAE Commission on Diagnostic Methods. Epilepsia 54:1315–1329. https://doi.org/10.1111/epi.12220
4. Brunne B, Zhao S, Derouiche A, Herz J, May P, Frotscher M, Bock HH (2010) Origin, maturation, and astroglial transformation of secondary radial glial cells in the developing dentate gyrus. Glia 58:1553–1569. https://doi.org/10.1002/glia.21029
5. Chazalon M, Paredes-Rodriguez E, Morin S, Martinez A, Cristovao-Ferreira S, Vaz S, Sebastiao A, Panatier A, Boue-Grabot E, Miguelez C et al (2018) GAT-3 dysfunction generates tonic inhibition in external globus pallidus neurons in Parkinsonian rodents. Cell Rep 23:1678–1690. https://doi.org/10.1016/j.celrep.2018.04.014
6. Chen I, Pant S, Wu Q, Cater RJ, Sobti M, Vandenberg RJ, Stewart AG, Tajkhorshid E, Font J, Ryan RM (2021) Glutamate transporters have a chloride channel with two hydrophobic gates. Nature 591:327–331. https://doi.org/10.1038/s41586-021-03240-9
7. Chivukula AS, Suslova M, Kortzak D, Kovermann P, Fahlke C (2020) Functional consequences of *SLC1A3* mutations associated with episodic ataxia 6. Hum Mutat 41:1892–1905. https://doi.org/10.1002/humu.24089
8. Choi KD, Jen JC, Choi SY, Shin JH, Kim HS, Kim HJ, Kim JS, Choi JH (2017) Late-onset episodic ataxia associated with *SLC1A3* mutation. J Hum Genet 62:443–446. https://doi.org/10.1038/jhg.2016.137
9. Choi KD, Kim JS, Kim HJ, Jung I, Jeong SH, Lee SH, Kim DU, Kim SH, Choi SY, Shin JH et al (2017) Genetic variants associated with episodic ataxia in Korea. Sci Rep 7:13855. https://doi.org/10.1038/s41598-017-14254-7
10. Coulter DA, Carlson GC (2007) Functional regulation of the dentate gyrus by GABA-mediated inhibition. Prog Brain Res 163:235–243. https://doi.org/10.1016/S0079-6123(07)63014-3
11. Danboldt NC (2001) Glutamate uptake. Prog Neurobiol 65:1–105. https://doi.org/10.1016/s0301-0082(00)00067-8
12. Davies CH, Pozza MF, Collingridge GL (1993) CGP 55845A: a potent antagonist of $GABA_B$ receptors in the CA1 region of rat hippocampus. Neuropharmacol 32:1071–1073. https://doi.org/10.1016/0028-3908(93)90073-c
13. de Vries B, Mamsa H, Stam AH, Wan J, Bakker SL, Vanmolkot KR, Haan J, Terwindt GM, Boon EM, Howard BD et al (2009) Episodic ataxia associated with EAAT1 mutation C186S affecting glutamate reuptake. Arch Neurol 66:97–101. https://doi.org/10.1001/archneurol.2008.535
14. Debanne D, Thompson SM, Gahwiler BH (2006) A brief period of epileptiform activity strengthens excitatory synapses in the rat hippocampus in vitro. Epilepsia 47:247–256. https://doi.org/10.1111/j.1528-1167.2006.00416.x
15. DeCarolis NA, Mechanic M, Petrik D, Carlton A, Ables JL, Malhotra S, Bachoo R, Gotz M, Lagace DC, Eisch AJ (2013) *In vivo* contribution of nestin- and GLAST-lineage cells to adult hippocampal neurogenesis. Hippocampus 23:708–719. https://doi.org/10.1002/hipo.22130
16. Dube CM, Ravizza T, Hamamura M, Zha Q, Keebaugh A, Fok K, Andres AL, Nalcioglu O, Obenaus A, Vezzani A et al (2010) Epileptogenesis provoked by prolonged experimental febrile seizures: mechanisms and biomarkers. J Neurosci 30:7484–7494. https://doi.org/10.1523/JNEUROSCI.0551-10.2010
17. Ehm O, Goritz C, Covic M, Schaffner I, Schwarz TJ, Karaca E, Kempkes B, Kremmer E, Pfrieger FW, Espinosa L et al (2010) RBPJkappa-dependent signaling is essential for long-term maintenance of neural stem cells in the adult hippocampus. J Neurosci 30:13794–13807. https://doi.org/10.1523/JNEUROSCI.1567-10.2010
18. Engels M, Kalia M, Rahmati S, Petersilie L, Kovermann P, van Putten M, Rose CR, Meijer HGE, Gensch T, Fahlke C (2021) Glial chloride homeostasis under transient ischemic stress. Front Cell Neurosci 15:735300. https://doi.org/10.3389/fncel.2021.735300
19. Fahlke C, Kortzak D, Machtens JP (2016) Molecular physiology of EAAT anion channels. Pflugers Arch Eur J Physiol 468:491–502. https://doi.org/10.1007/s00424-015-1768-3
20. Fairman WA, Vandenberg RJ, Arriza JL, Kavanaugh MP, Amara SG (1995) An excitatory amino-acid transporter with properties of a ligand-gated chloride channel. Nature 375:599–603. https://doi.org/10.1038/375599a0
21. Farrant M, Nusser Z (2005) Variations on an inhibitory theme: phasic and tonic activation of GABA(A) receptors. Nat Rev Neurosci 6:215–229. https://doi.org/10.1038/nrn1625
22. Feng HJ, Kang JQ, Song L, Dibbens L, Mulley J, Macdonald RL (2006) δ subunit susceptibility variants E177A and R220H associated with complex epilepsy alter channel gating and surface expression of $\alpha4\beta2\delta GABA_A$ receptors. J Neurosci 26:1499–1506. https://doi.org/10.1523/JNEUROSCI.2913-05.2006
23. Grote A, Heiland DH, Taube J, Helmstaedter C, Ravi VM, Will P, Hattingen E, Schure JR, Witt JA, Reimers A et al (2023) "Hippocampal innate inflammatory gliosis only" in pharmacoresistant temporal lobe epilepsy. Brain 146:549–560. https://doi.org/10.1093/brain/awac293
24. Hattingen E, Enkirch SJ, Jurcoane A, Kruse M, Delev D, Grote A, Becker A (2018) Hippocampal "gliosis only" on MR imaging represents a distinct entity in epilepsy patients. Neuroradiology 60:161–168. https://doi.org/10.1007/s00234-017-1939-3
25. Holter NI, Zylla MM, Zuber N, Bruehl C, Draguhn A (2010) Tonic GABAergic control of mouse dentate granule cells during postnatal development. Eur J Neurosci 32:1300–1309. https://doi.org/10.1111/j.1460-9568.2010.07331.x
26. Hotzy J, Schneider N, Kovermann P, Fahlke C (2013) Mutating a conserved proline residue within the trimerization domain modifies Na^+ binding to excitatory amino acid transporters and associated conformational changes. J Biol Chem 288:36492–36501. https://doi.org/10.1074/jbc.M113.489385
27. Iwama K, Iwata A, Shiina M, Mitsuhashi S, Miyatake S, Takata A, Miyake N, Ogata K, Ito S, Mizuguchi T et al (2017) A novel mutation in *SLC1A3* causes episodic ataxia. J Hum Genet 63:207–211. https://doi.org/10.1038/s10038-017-0365-z
28. Jen JC, Wan J, Palos TP, Howard BD, Baloh RW (2005) Mutation in the glutamate transporter EAAT1 causes episodic ataxia, hemiplegia, and seizures. Neurology 65:529–534. https://doi.org/10.1212/01.wnl.0000172638.58172.5a
29. Joshi S, Rajasekaran K, Sun H, Williamson J, Kapur J (2017) Enhanced AMPA receptor-mediated neurotransmission on CA1 pyramidal neurons during status epilepticus. Neurobiol Dis 103:45–53. https://doi.org/10.1016/j.nbd.2017.03.017
30. Jungblut M, Tiveron MC, Barral S, Abrahamsen B, Knobel S, Pennartz S, Schmitz J, Perraut M, Pfrieger FW, Stoffel W et al (2012) Isolation and characterization of living primary astroglial cells using the new GLAST-specific monoclonal antibody ACSA-1. Glia 60:894–907. https://doi.org/10.1002/glia.22322
31. Kanai Y, Hediger MA (2004) The glutamate/neutral amino acid transporter family SLC1: molecular, physiological and pharmacological aspects. Pflugers Arch Eur J Physiol 447:469–479. https://doi.org/10.1007/s00424-003-1146-4
32. Kaneko H, Putzier I, Frings S, Kaupp UB, Gensch T (2004) Chloride accumulation in mammalian olfactory sensory neurons. J Neurosci 24:7931–7938. https://doi.org/10.1523/JNEUROSCI.2115-04.2004

33. Kavanaugh MP, Arriza JL, North RA, Amara SG (1992) Electrogenic uptake of gamma-aminobutyric acid by a cloned transporter expressed in *Xenopus* oocytes. J Biol Chem 267:22007–22009
34. Kovermann P, Bayat A, Fenger CD, Leeuwen L, Borovikov A, Sharkov A, Levrat V, Lesca G, Perrin L, Levy J et al (2025) The severity of *SLC1A2* associated neurodevelopmental disorders correlates with transporter dysfunction. EBioMedicine. https://doi.org/10.1016/j.ebiom.2025.105648
35. Kovermann P, Engels M, Müller F, Fahlke C (2022) Cellular physiology and pathophysiology of EAAT anion channels. Front Cell Neurosci 15:815279. https://doi.org/10.3389/fncel.2021.815279
36. Kovermann P, Kolobkova Y, Franzen A, Fahlke C (2022) Mutations associated with epileptic encephalopathy modify EAAT2 anion channel function. Epilepsia 63:388–401. https://doi.org/10.1111/epi.17154
37. Kovermann P, Untiet V, Kolobkova Y, Engels M, Baader S, Schilling K, Fahlke C (2020) Increased glutamate transporter-associated anion currents cause glial apoptosis in episodic ataxia 6. Brain Commun. https://doi.org/10.1093/braincomms/fcaa022
38. Krapf R, Berry CA, Verkman AS (1988) Estimation of intracellular chloride activity in isolated perfused rabbit proximal convoluted tubules using a fluorescent indicator. Biophys J 53:955–962. https://doi.org/10.1016/S0006-3495(88)83176-X
39. Langer J, Rose CR (2009) Synaptically induced sodium signals in hippocampal astrocytes *in situ*. J Physiol 587:5859–5877. https://doi.org/10.1113/jphysiol.2009.182279
40. Larsson HP, Picaud SA, Werblin FS, Lecar H (1996) Noise analysis of the glutamate-activated current in photoreceptors. Biophys J 70:733–742. https://doi.org/10.1016/S0006-3495(96)79613-3
41. Lu CC, Hilgemann DW (1999) GAT1 (GABA:Na^+:Cl^-) cotransport function. Steady state studies in giant *Xenopus* oocyte membrane patches. J Gen Physiol 114:429–444. https://doi.org/10.1085/jgp.114.3.429
42. Machtens JP, Kortzak D, Lansche C, Leinenweber A, Kilian P, Begemann B, Zachariae U, Ewers D, de Groot BL, Briones R et al (2015) Mechanisms of anion conduction by coupled glutamate transporters. Cell 160:542–553. https://doi.org/10.1016/j.cell.2014.12.035
43. Maguire JL, Stell BM, Rafizadeh M, Mody I (2005) Ovarian cycle-linked changes in $GABA_A$ receptors mediating tonic inhibition alter seizure susceptibility and anxiety. Nat Neurosci. https://doi.org/10.1038/nn1469
44. Meurs A, Clinckers R, Ebinger G, Michotte Y, Smolders I (2008) Seizure activity and changes in hippocampal extracellular glutamate, GABA, dopamine and serotonin. Epilepsy Res 78:50–59. https://doi.org/10.1016/j.eplepsyres.2007.10.007
45. Mitchell SJ, Silver RA (2003) Shunting inhibition modulates neuronal gain during synaptic excitation. Neuron 38:433–445. https://doi.org/10.1016/s0896-6273(03)00200-9
46. Moss J, Gebara E, Bushong EA, Sanchez-Pascual I, O'Laoi R, El M'Ghari I, Kocher-Braissant J, Ellisman MH, Toni N (2016) Fine processes of Nestin-GFP-positive radial glia-like stem cells in the adult *dentate gyrus* ensheathe local synapses and vasculature. PNAS 113:E2536-2545. https://doi.org/10.1073/pnas.1514652113
47. Richards DA, Mateos JM, Hugel S, de Paola V, Caroni P, Gahwiler BH, McKinney RA (2005) Glutamate induces the rapid formation of spine head protrusions in hippocampal slice cultures. Proc Natl Acad Sci U S A 102:6166–6171. https://doi.org/10.1073/pnas.0501881102
48. Risher WC, Ustunkaya T, Singh Alvarado J, Eroglu C (2014) Rapid Golgi analysis method for efficient and unbiased classification of dendritic spines. PLoS ONE 9:e107591. https://doi.org/10.1371/journal.pone.0107591
49. Rose CR, Ziemens D, Untiet V, Fahlke C (2018) Molecular and cellular physiology of sodium-dependent glutamate transporters. Brain Res Bull 136:3–16. https://doi.org/10.1016/j.brainresbull.2016.12.013
50. Rothstein JD, Martin L, Levey AI, Dykes-Hoberg M, Jin L, Wu D, Nash N, Kuncl RW (1994) Localization of neuronal and glial glutamate transporters. Neuron 13:713–725. https://doi.org/10.1016/0896-6273(94)90038-8
51. Salah A, Perkins KL (2008) Effects of subtype-selective group I mGluR antagonists on synchronous activity induced by 4-aminopyridine/CGP 55845 in adult guinea pig hippocampal slices. Neuropharmacol 55:47–54. https://doi.org/10.1016/j.neuropharm.2008.04.010
52. Semyanov A, Walker MC, Kullmann DM (2003) GABA uptake regulates cortical excitability via cell type-specific tonic inhibition. Nat Neurosci 6:484–490. https://doi.org/10.1038/nn1043
53. Shigetomi E, Tong X, Kwan KY, Corey DP, Khakh BS (2011) TRPA1 channels regulate astrocyte resting calcium and inhibitory synapse efficacy through GAT-3. Nat Neurosci 15:70–80. https://doi.org/10.1038/nn.3000
54. Sofroniew MV, Vinters HV (2010) Astrocytes: biology and pathology. Acta Neuropathol 119:7–35. https://doi.org/10.1007/s00401-009-0619-8
55. Spigelman I, Li Z, Banerjee PK, Mihalek RM, Homanics GE, Olsen RW (2002) Behavior and physiology of mice lacking the $GABA_A$-receptor δ subunit. Epilepsia 43. Suppl 5:3–8. https://doi.org/10.1046/j.1528-1157.43.s.5.8.x
56. Stoffel W, Korner R, Wachtmann D, Keller BU (2004) Functional analysis of glutamate transporters in excitatory synaptic transmission of GLAST1 and GLAST1/EAAC1 deficient mice. Brain Res Mol Brain Res 128:170–181. https://doi.org/10.1016/j.molbrainres.2004.06.026
57. Suslova M, Kortzak D, Machtens JP, Kovermann P, Fahlke C (2023) Apo state pore opening as functional basis of increased EAAT anion channel activity in episodic ataxia 6. Front Physiol 14:1147216. https://doi.org/10.3389/fphys.2023.1147216
58. Untiet V, Kovermann P, Gerkau NJ, Gensch T, Rose CR, Fahlke C (2017) Glutamate transporter-associated anion channels adjust intracellular chloride concentrations during glial maturation. Glia 65:388–400. https://doi.org/10.1002/glia.23098
59. Vandenberg RJ, Ryan RM (2013) Mechanisms of glutamate transport. Physiol Rev 93:1621–1657. https://doi.org/10.1152/physrev.00007.2013
60. Verkman AS (1990) Development and biological applications of chloride-sensitive fluorescent indicators. Am J Physiol 259:C375-388
61. Vezzani A, Moneta D, Conti M, Richichi C, Ravizza T, De Luigi A, De Simoni MG, Sperk G, Andell-Jonsson S, Lundkvist J et al (2000) Powerful anticonvulsant action of IL-1 receptor antagonist on intracerebral injection and astrocytic overexpression in mice. Proc Natl Acad Sci U S A 97:11534–11539. https://doi.org/10.1073/pnas.190206797
62. Watase K, Hashimoto K, Kano M, Yamada K, Watanabe M, Inoue Y, Okuyama S, Sakagawa T, Ogawa S, Kawashima N et al (1998) Motor discoordination and increased susceptibility to cerebellar injury in GLAST mutant mice. Eur J Neurosci 10:976–988
63. Winter N, Kovermann P, Fahlke C (2012) A point mutation associated with episodic ataxia 6 increases glutamate transporter anion currents. Brain 135:3416–3425. https://doi.org/10.1093/brain/aws255
64. Wlodarczyk AI, Sylantyev S, Herd MB, Kersante F, Lambert JJ, Rusakov DA, Linthorst AC, Semyanov A, Belelli D, Pavlov I et al (2013) GABA-independent $GABA_A$ receptor openings maintain tonic currents. J Neurosci 33:3905–3914. https://doi.org/10.1523/JNEUROSCI.4193-12.2013
65. Wu Q, Akhter A, Pant S, Cho E, Zhu JX, Garner A, Ohyama T, Tajkhorshid E, van Meyel DJ, Ryan RM (2022) Ataxia-linked *SLC1A3* mutations alter EAAT1 chloride channel activity and glial regulation of CNS function. J Clin Invest 132:e154891. https://doi.org/10.1172/JCI154891
66. Zilles K, Palomero-Gallagher N, Grefkes C, Scheperjans F, Boy C, Amunts K, Schleicher A (2002) Architectonics of the human cerebral cortex and transmitter receptor fingerprints: reconciling functional neuroanatomy and neurochemistry. Eur Neuropsychopharmacol 12:587–599. https://doi.org/10.1016/s0924-977x(02)00108-6
67. Zipfel WR, Williams RM, Webb WW (2003) Nonlinear magic: multiphoton microscopy in the biosciences. Nat Biotechnol 21:1369–1377. https://doi.org/10.1038/nbt899
68. Zolkowska D, Banks CN, Dhir A, Inceoglu B, Sanborn JR, McCoy MR, Bruun DA, Hammock BD, Lein PJ, Rogawski MA (2012) Characterization of seizures induced by acute and repeated exposure to tetramethylenedisulfotetramine. J Pharmacol Exp Ther 341:435–446. https://doi.org/10.1124/jpet.111.190579

Publisher's Note